Science of the Total Environment 714 (2020) 136867

Contents lists available at ScienceDirect

Science of the Total Environment

journal homepage: www.elsevier.com/locate/scitotenv

Application of isotopic and geochemical signals in unconventional oil and gas reservoir produced waters toward characterizing in situ geochemical fluid-shale reactions

Thai T. Phan [a,b,c,*], J. Alexandra Hakala [a], Shikha Sharma [d]

[a] National Energy Technology Laboratory, U.S. Department of Energy, Pittsburgh, PA 15236, USA
[b] Department of Geology and Environmental Science, University of Pittsburgh, Pittsburgh, PA 15260, USA
[c] Department of Earth and Environmental Sciences, University of Waterloo, Waterloo, ON N2L 3G1, Canada
[d] Department of Geology and Geography, West Virginia University, Morgantown, WV 26506, USA

HIGHLIGHTS

- Sr/Na, Ca/Na, B/Na, and $^{87}Sr/^{86}Sr$ of early produced water (PW) reflects carbonate dissolution.
- Elevated trace metal contents suggest oxidation of sulfide minerals by fracturing chemicals.
- ^{6}Li enriched early PW is due to desorption of ^{6}Li from clays and organic matter.
- Change in PW chemistry is a result of mixing between fracturing fluid and local formation water.
- Fractured reservoir under oxidizing condition during fracturing period moves toward reducing environment during production.

GRAPHICAL ABSTRACT

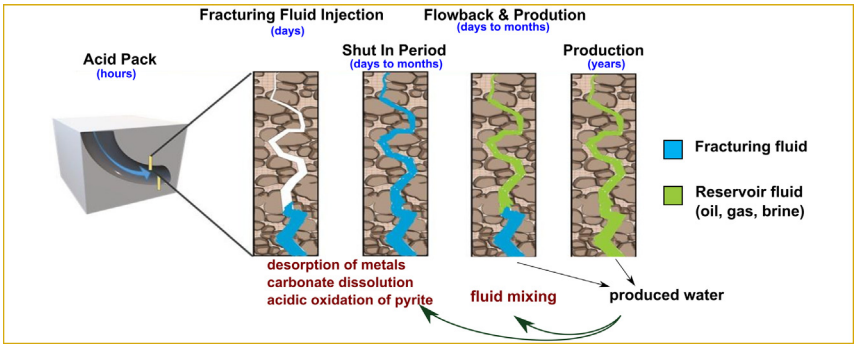

ARTICLE INFO

Article history:
Received 31 October 2019
Received in revised form 12 January 2020
Accepted 21 January 2020
Available online 23 January 2020

Editor: Yolanda Picó

Keywords:
Produced water
Isotopic tracers
Water-rock interactions
Trace metals
Marcellus Shale

ABSTRACT

Optimizing hydrocarbon production and waste management from unconventional oil and gas extraction requires an understanding of the fluid-rock chemical interactions. These reactions can affect flow pathways within fractured shale and produced water chemistry. Knowledge of these chemical reactions also provides valuable information for planning wastewater treatment strategies. This study focused on characterizing reservoir reactions through analysis of produced water chemistry from the Marcellus Shale Energy and Environmental Laboratory field site in Morgantown, WV, USA. Analysis of fracturing fluids, time-series produced waters (PW) over 16 months of operation of two hydraulically fractured gas wells, and shale rocks from the same well for metal concentrations and multiple isotope signatures ($\delta^{2}H$ and $\delta^{18}O$ of water, $\delta^{7}Li$, $\delta^{11}B$, $^{87}Sr/^{86}Sr$) showed that the chemical and isotopic composition of early (<10 days) PW samples record water-rock interactions during the fracturing period. Acidic dissolution of carbonate minerals was evidenced by the increase in TOC, B/Na, Sr/Na, Ca/Na, and the decrease in $^{87}Sr/^{86}Sr$ in PW returning in the first few days toward the $^{87}Sr/^{86}Sr$ signature of carbonate cement. The enrichment of ^{6}Li in these early (e.g., day 1) PW samples is most likely a result of desorption of Li from clays and organic matter due to the injection of fracturing fluid. Redox-active trace elements appear to be controlled by oxidation-reduction reactions and potentially reactions involving wellbore steel. Overall, PW chemistry is primarily controlled by mixing between early PW with local in-situ formation water however

* Corresponding author at: Department of Earth and Environmental Sciences, University of Waterloo, Waterloo, ON N2L 3G1, Canada
E-mail address: thai.phan@uwaterloo.ca (T.T. Phan).

https://doi.org/10.1016/j.scitotenv.2020.136867

certain geochemical reactions (e.g., carbonate cement dissolution and desorption of ^{6}Li from clays and organic matter) can be inferred from PW composition monitored immediately over the first ten days of water return.

1. Introduction

Hydraulic fracturing technology used for the recovery of natural gas from tight organic rich shales in the United States has garnered immense interest in global development of this unconventional energy resource. Ensuring the availability of oil and gas from hydraulically-fractured unconventional reservoirs requires knowledge of reservoir processes that affect both hydrocarbon production, and the management of produced water. Hydrocarbon production from these resources is high during the first year of production, however, declines rapidly in later years (Ghahfarokhi et al., 2018; Patzek et al., 2013). Laboratory-based studies on fracturing fluid-shale reactions indicate that dissolution of primary shale minerals and precipitation of secondary minerals within the shale matrix and fractures, and clay swelling, can block hydrocarbon flow pathways from the fractured reservoir (Civan, 2015; Jew et al., 2017; Marcon et al., 2017; Paukert Vankeuren et al., 2017; Pearce et al., 2018). Restriction of hydrocarbon flow within the reservoir can negatively affect production. Concerns about produced water affecting surface waters and sediments (Burgos et al., 2017; Orem et al., 2017; Warner et al., 2013), and the potential to treat produced water streams for beneficial use (Wenzlick et al., 2018), also warrant an understanding of in situ reservoir processes that control produced water composition.

Water injected during hydraulic fracturing can directly interact with shale in the reservoir by dissolving and precipitating minerals and/or by mobilizing pore fluids and in situ brines. Low TDS (usually <50,000 mg/L) water is used as the base fluid for fracturing fluids, and comprises mainly freshwater or a mixture of freshwater and produced water from previous wells (King, 2012). Chemicals, such as scale inhibitors, friction reducers, and biocides, are added to the base water to create the hydraulic fracturing fluid (King, 2012). After hydraulic fracturing, an average of 10–25% of the injected water volume returns to the surface during the first two weeks following a decrease in borehole pressures (Haluszczak et al., 2013; Osselin et al., 2018). This water primarily contains fracturing fluid and highly saline formation water (Blauch et al., 2009; Cluff et al., 2014; Osselin et al., 2018; Phan et al., 2016; Rowan et al., 2015). In this study, the early return fluid (<10 days) is referred to as "early PW". Depending on the operation of the well, the composition of the produced water shifts from the primarily hydraulic fracturing fluid toward the composition of formation water. This transition can occur within the first two months (Phan et al., 2016) or up to a year (Rowan et al., 2015). Using organic sulfur as a tracer, Luek et al. (2018) showed that fracturing chemicals could remain in the reservoir for up to 10 months since injection. The chemical composition of the early PW depends not only on the composition of the hydraulic fracturing fluid and the shale rock but also on the residence time of the fluid in the reservoir. Geochemically, the early PW will retain the signatures of their respective sources and additives, and produced water at later stage of production will exhibit signatures of the native formation waters (Capo et al., 2014; Phan et al., 2016; Rowan et al., 2015; Sharma et al., 2015).

While Marcellus Shale PW contains high Ra (Rowan et al., 2011), its U concentration is extremely low (<0.1 μg/L), probably due to the anoxic conditions in the subsurface (Phan et al., 2015). The anoxic conditions have also been inferred by the presence of anaerobic bacteria in the PW (Akob et al., 2015). Deoxygenation of the fracturing fluid before injection into the hydrocarbon-bearing reservoir is not regularly performed. For example, a high level of dissolved oxygen (~9 mg/L) was found in early produced waters from the Horn River Basin (Zolfaghari et al., 2016). More importantly, oxidants added in the fracturing fluid could trigger the oxidation of shale minerals such as pyrite (Jew et al., 2017). These studies clearly indicate that the changes in the redox conditions during fracturing and the lifespan of a gas well could trigger oxidation/reduction reactions resulting in dissolution/precipitation of minerals in the fractured reservoir.

Most of the current water-rock interactions studies related to hydraulic fracturing of shales rely on experimental approaches (Harrison et al., 2017; Jew et al., 2017; Marcon et al., 2017; Ouyang et al., 2017; Ouyang et al., 2018; Paukert Vankeuren et al., 2017; Pearce et al., 2018; Phan et al., 2018b; Pilewski et al., 2019; Renock et al., 2016; Stewart et al., 2015; Tasker et al., 2016) mainly because mixing with in situ hypersaline formation water (Capo et al., 2014; Phan et al., 2016) overwhelms geochemical changes induced by water-rock interactions (Phan et al., 2018b). For example, Paukert Vankeuren et al. (2017) experimentally demonstrated that oxidation of pyrite and ammonium persulfate, a gel breaker, releases sulfate leading to barite formation that affects reservoir permeability. Similarly, precipitation of secondary minerals such as Al- and Fe-bearing phases (Harrison et al., 2017; Marcon et al., 2017; Pearce et al., 2018) could cause clogging of pores and fracture apertures. Calcite dissolution is also an important reaction because this reaction could release U into PW (Phan et al., 2018b), increasing porosity of the reservoir (Harrison et al., 2017; Paukert Vankeuren et al., 2017), buffering pH, thus suppressing the oxidation of pyrite (Jew et al., 2017); however, the latter might not be the case for Marcellus Shale because of its low buffering capacity in comparison to other high carbonaceous shales such as Green River and Eagle Ford (Jew et al., 2017). To this note, the dissolution of carbonate cement in Marcellus Shale does not affect the temporal change in $\delta^{7}Li$ in produced water because Li abundance is low in the carbonate minerals (Phan et al., 2016). To date, complex geochemical reactions in hydraulically fractured reservoirs still demand further understanding which is critical to designing effective fracturing fluid and managing produced water treatment and disposal.

To better understand the water-rock interactions in the reservoir that can affect hydrocarbon flow and to better evaluate the human-ecological health risks associated with the storage, transport, and treatment of produced water it is essential to know the temporal changes in the produced water composition (Capo et al., 2014; Osselin et al., 2019; Phan et al., 2016; Rosenblum et al., 2017). Dissolved inorganic constituents that can be used to track fluid-rock reaction versus fluid mixing reactions are naturally present in PW from Marcellus Shale (Haluszczak et al., 2013; Phan et al., 2015; Rowan et al., 2011).

In this study, we evaluated the downhole geochemical reactions and fluid mixing in the shale reservoir by characterizing the fracturing fluids, and 16-month time-series produced water samples collected from two Marcellus Shale gas wells at a research site in Morgantown, WV, USA. We have used the term "produced water" (PW) for all the water returning from the wellhead regardless of the time post-hydraulic fracturing (Capo et al., 2014; Phan et al., 2015; Rowan et al., 2015) and the term "early PW" is used for the PW recovered during the initial days (<10 days) of production. To broaden the geochemical signals that may be applied to distinguish fluid-rock reactions in the reservoir, we applied multiple isotope proxies ($\delta^{2}H$, $\delta^{18}O$, $\delta^{7}Li$, $\delta^{11}B$, $^{87}Sr/^{86}Sr$) in addition to inorganic constituents of both PW and Marcellus Shale source rock to provide a comprehensive understanding of water-rock reactions occurring in situ. This study is unique because both the PW and rock samples were collected from the same

hydraulically fractured Marcellus gas well, enabling a better understanding of the chemical reactions that take place in the shale reservoir after the introduction of hydraulic fracturing fluids.

2. Methods

2.1. Study area and samples

2.1.1. Time-series produced water samples

Time-series PW samples ($n = 54$) were collected over a period of 16 months from two hydraulically fractured Marcellus Shale gas wells (MIP-3H and MIP-5H) from the Marcellus Shale Energy and Environment Laboratory (MSEEL) field site in Monongalia County, WV, USA (Fig. 1). In addition, "fracturing fluid" samples (3H-FF and 5H-FF) from stage 11 of the 28 hydraulic fracturing stages of MIP-3H and MIP-5H and a water sample (make-up water) from Monongahela river were also analyzed (Table 1). The fracturing fluids are the clean fluids used in stage 11 which comprise of fracturing chemicals (unknown names and compositions) and primarily freshwater from nearby Monongalia river, facilitating the application of geochemical tracers in understanding potential reservoir reactions. These fracturing fluids primarily represent the make-up water, which is from Monongahela river. Well MIP-3H and MIP-5H were hydraulically fractured from November 6th to 15th 2015 and from October 28th to November 5th 2015, respectively. The total injected fluid into MIP-3H well was about 40,307 m^3 whereas only 2250 m^3 PW (5.6% of the injected fluid) was recovered within 16 months of production. The produced water samples were collected from gas-water separators following the procedure described in detail in Phan et al. (2018a), a typical procedure (Kharaka et al., 1987) commonly used to collect PW from oil and gas wells (Engle et al., 2016; Pfister et al., 2017; Rowan et al., 2015). In this study, the aqueous phase was separated from oil in the laboratory at the West Virginia University within an hour after collecting from the MSEEL field site by letting the sample sit for at least an hour, pre-filtered through glass wool, and then filtered through a high capacity in-line 0.45 μm filter cartridge. The pre-filtered water was discarded before sampling PW. Samples for major and trace metals were preserved with ultra-pure nitric acid (Optima® grade). Samples for anion concentration analysis were further filtered through a 0.2 μm membrane and stored at 4 °C.

2.1.2. Leachates of drill core materials of Marcellus Shale

It is important to know the geochemical compositions of bulk and leachable fractions of the host rock to facilitate understanding of chemical reactions occurring in the formation. Therefore, leachates of Marcellus Shale rocks ($n = 35$) recovered from a drill core (MIP-3H, 39°36′06.5″N 79°58′34.0″W), the same well in which time-series PW samples were collected, were used in this study. These core samples cover the entire Marcellus Shale: both Oatka Creek and Union Springs members.

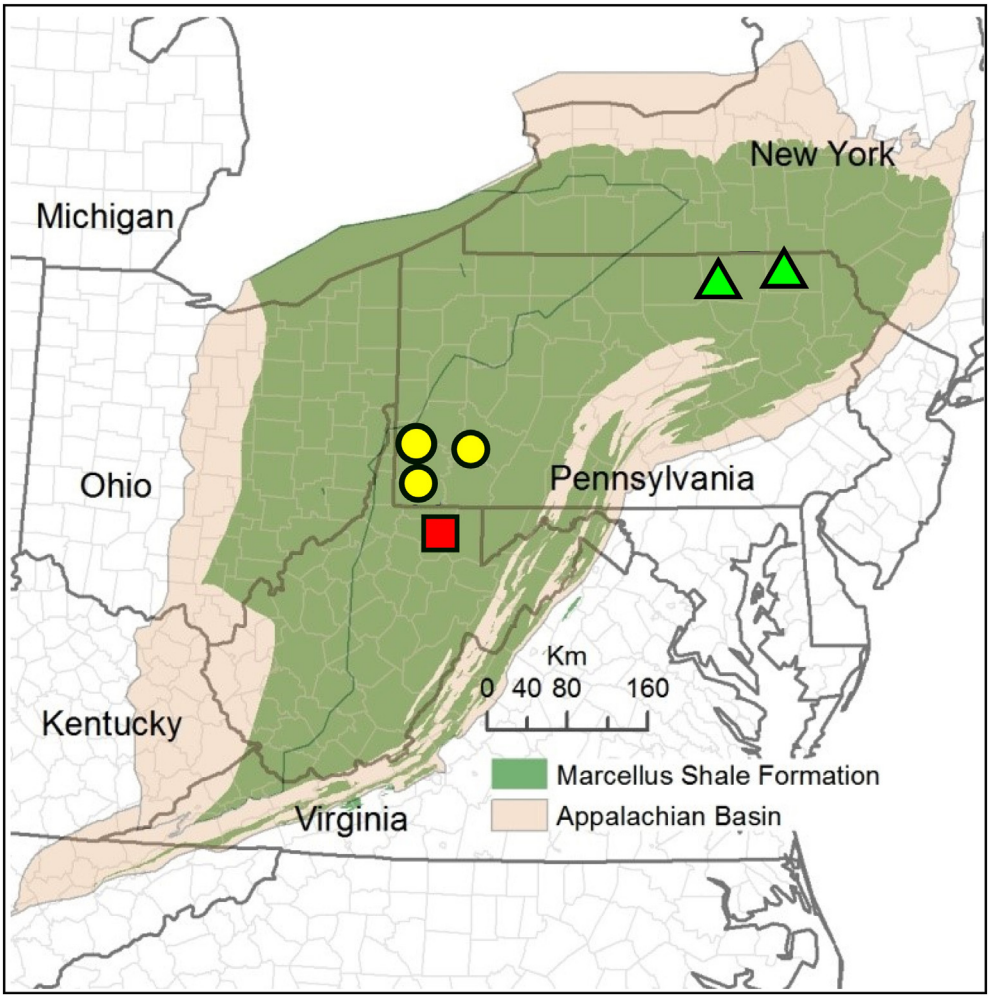

Fig. 1. Time-series PW samples reported in this study were collected from two gas wells in the Marcellus Shale Energy and Environment Laboratory (MSEEL) field site in Monongalia County, WV, USA (rectangle). Additional PW data (Capo et al., 2014; Chapman et al., 2012; Phan et al., 2016; Rowan et al., 2015) from southwestern PA (circles) and northcentral PA (triangles) are also used for comparison. Present-day Marcellus Shale base map is modified after Whitacre (2014).

Table 1
Isotope data (δ^2H, $\delta^{18}O$, δ^7Li, $\delta^{11}B$, $^{87}Sr/^{86}Sr$,) of fracturing fluid and produced waters of Marcellus Shale in Monongalia Co., WV, USA.

Sample ID	Production time	Cumulated volume	TOC	TDS[a]	$\delta^2H_{V\text{-}SMOW}$	$\delta^{18}O_{V\text{-}SMOW}$	δ^7Li	±2SD[b] ($n = 2$)	$\delta^{11}B$	±2SD[b] ($n = 2$)	$^{87}Sr/^{86}Sr$	±2SD[b] ($n = 3$)	ε_{Sr}	±2SD[b,c] ($n = 3$)
	day	m^3	mg/L	mg/L			‰		‰					
Well MIP-3H (longtitude = 39.601783, latitude = −79.976123)														
Make-up water[e]					−48.1	−8.7								
3H-FF			6	300			24.3	1.1			0.711916	0.000003	39	0.04
3H-01[d]	1.0	131	66	23,800	−38	−6.3	9.6	0.2	28.5	0.3	0.711114	0.000006	27	0.08
3H-02	1.3		77	24,500	−45	−5.6	na		28.1	0.7	0.711071	0.000009	27	0.13
3H-03[d]	2.0	417	90	25,000	−44	−5.5	9.1	1.3	27.6	0.1	0.711041	0.000015	26	0.21
3H-04[d]	2.3		234	68,600	−38	−4.7	11	0.4	27.2	0.1	0.710434	0.000042	18	0.60
3H-05	2.5		120	36,400	−41	−5.4	na		28.0		0.710684	0.000039	21	0.55
3H-06	2.8		119	37,600	−41	−5.1	9.9	0.2	27.9	0.0	0.710687		21	
3H-07[d]	3.0	638	211	72,000	−38	−4.5	10	0.4	27.7	0.6	0.710426		18	
3H-08	3.3		105	30,900	−45	−5.1	na		28.1	0.4	0.711020		26	
3H-09	3.6		104	31,600	−42	−5.1	na		28.5	0.2	0.710978		26	
3H-10[d]	4.0	813	105	35,400	−31	−4.9	9.5	0.8	28.6	1.0	0.711041		26	
3H-11[d]	5.0	920	110	39,200	−40	−4.8	na				0.711113		27	
3H-12[d]	6.0	988	94	42,400	−38	−4.8	na				0.711182		28	
3H-13[d]	7.0	1017	91	45,200	−43	−4.7	na				0.711222		29	
3H-14[d]	9.0	1074	84	49,500	−45	−4.7	na				0.711283		30	
3H-15[d]	10	1097	86	51,500	−41	−4.7	na		29.4	1.0	0.711234		29	
3H-16[d]	11	1111	83	52,800	−41	−4.6	na				0.711256		29	
3H-17[d]	12	1123	81	54,300	−39	−4.7	na				0.711278		30	
3H-18[d]	13	1134	78	54,300	−42	−4.7	10	0.2	30.0	0.7	0.711303		30	
3H-19[d]	21	1247	111	67,200	−39	−3.4	na		29.7		0.711248		29	
3H-20[d]	36	1430	na	75,400	−42	−4.3	na		29.8	0.2	0.711300		30	
3H-21[d]	56	1561	na	92,900	−37	−4.2	na		30.2	0.1	0.711339		31	
3H-22	69	1655	58	110,700	−39	−4.0	na				0.711312		30	
3H-23	118	1763	58	118,200	−36	−3.7	11.1	0.0	30.1	0.2	0.711293		30	
3H-24	148	1831	49	129,300	−35	−3.5	na				0.711334	0.000012	31	0.2
3H-25	181	1850	60	107,400	−42	−4.4	na				0.711308		30	
3H-26	216	1861	47	131,200	na	na	na				0.711316		30	
3H-27	279	1867	50	119,100	na	na	11.7	0.8	30.1	0.6	0.711305	0.000038	30.2	0.5
3H-28	405	2015	275	153,000	na	na	na		30.1	0.9	0.711276		29.8	
3H-29	461	2199	131	145,400	na	na	na		29.5	0.7	0.711161		28.1	
3H-30	489	2250	57	157,700	na	na	11.9	1.1	29.5	0.8	0.711301	0.000007	30.1	0.1
Well MIP-5H (longtitude = 39.601833, latitude = −79.976152)														
Make-up water[e]					−48.1	−8.7								
5H-FF			6	300			24.4	0.4	na		0.711897	0.000014	39	0.2
5H-01	1.0	157		68,400			11.0		na		0.710326		16	
5H-02	1.3			58,300	−36.4	−4.7	na		na		0.710481		19	
5H-03	2.0	368		56,000	−36.2	−4.7	9.9		na		0.710512		19	
5H-04	2.3			52,500			na		na		0.710590		20	
5H-05	2.5			55,300	−40.7	−4.5	na		na		0.710595		20	
5H-06	2.8			38,100	−43.6	−4.9	na		na		0.710963		25	
5H-07	3.0	434		38,900	−42.4	−4.9	9.7		na		0.711032		26	
5H-08	3.3			38,800	−39.8	−4.8	na		na		0.711081		27	
5H-09	3.6			42,800	−41.0	−4.5	na		na		0.711142		28	
5H-10	9.0	486		43,900	−38.9	−4.5	na		na		0.711205		29	
5H-11	10	503		43,200	−42.6	−4.3	9.5		na		0.711225		29	
5H-12	12	522		46,000	−41.0	−4.9	na		na		0.711281		30	
5H-13	13	530		48,000	−40.9	−4.5	na		na		0.711271		30	
5H-14	36	673		46,600	−37.9	−4.6	na		na		0.711161		28	
5H-15	56	804		66,400	−38.6	−4.2	10.5		na		0.711195		29	
5H-16	69	894	40	86,000			na		na		0.711192		29	
5H-17	83	947	32	100,800	−36.9	−3.8	na		na		0.711204		29	
5H-18	118	1017	35	98,200	−39.1	−3.9	na		na		0.711194	0.000027	29	0.4
5H-19	148	1088	41	111,800	−32.6	−3.4	na		na		0.711209		29	
5H-20	181	1109	31	125,500	−30.6	−4.4	na		na		0.711180		28	
5H-21	216	1119	25	96,600	na	na	na		na		0.711206		29	
5H-22	279	1124	30	116,300	na	na	na		na		0.711190	0.000005	29	0.1
5H-23	337	1142	33	102,800	na	na	na		na		0.711158		28	
5H-24	461	1282	984	248,200	na	na	11.6		na		0.711148	0.000008	28	0.1

[a] Calculated based on total concentrations of major cations and anions, excluding bi-carbonate.
[b] Two standard deviations of full analytical procedures (separated aliquots of the same samples were independently processed through column chemistry (δ^7Li and $^{87}Sr/^{86}Sr$) or sublimation ($\delta^{11}B$) and analyzed by MC-ICP-MS). Typical precisions on duplicate measurement of δ^7Li and $\delta^{11}B$ are about 0.2‰ and 0.5‰ on average, respectively.
[c] $\varepsilon^{Sr} = (^{87}Sr/^{86}Sr_{sample}/^{87}Sr/^{86}Sr_{seawater} - 1)10^4$ where $^{87}Sr/^{86}Sr_{seawater} = 0.709166$ (Chapman et al., 2012).
[d] TOC contents and $^{87}Sr/^{86}Sr$ of these samples were previously reported in Phan et al. (2018a).
[e] Make-up water is Monongahela river water that was used to mix fracturing fluids (3H-FF and 5H-FF).

These leachate samples are archived from a previous study (Procedure A in Phan et al., 2019). Briefly, the rock powder was sequentially extracted by (1) Milli-Q water (water/rock = 20) to extract water-soluble salts, (2) ammonium acetate pH 8 (water/rock = 40) to extract absorbed metals on organic matter and clay minerals, and (3) 1.0 N acetic acid (water/rock = 40) to extract metals associated with carbonate minerals. As shown in Table 2, this study reports the concentrations of Li, B, Cl, Br in these leachates in addition to Sr and $^{87}Sr/^{86}Sr$ which were previously reported in Phan et al. (2019).

2.2. Analytical methods

2.2.1. TOC, cation and anion concentrations

Total organic carbon (TOC) in the <0.45 μm filtered water and anion concentrations in the <0.2 μm filtered water were analyzed at the National Energy Technology Laboratory (NETL) in Pittsburgh, PA, USA. The TOC was measured by a Shimadzu TOC-L following the protocol for non-purgeable organic carbon (Table 1). Major anion concentrations were measured by ion chromatography (IC) Thermo Scientific™ Dionex™ ICS-5000+. The metal concentrations and total S were analyzed by inductively coupled plasma optical emission spectroscopy (ICP-OES) at NETL and by inductively coupled plasma mass spectrometry (ICP-MS; PerkinElmer NexION 300X) under kinetic energy discrimination (KED) mode at the University of Pittsburgh, as indicated in Table S1. A previous study (Tasker et al., 2019) showed that low concentrations of trace metals and large dilution of PW due to high TDS level apparently affect the accuracy of trace metal analysis. In this study, significant dilution of PW samples was done to achieve TDS level < 0.2% and indium was used as an internal standard for the correction of matrix effect during ICP-MS analysis. Some samples were also analyzed for major cations by IC as duplicate. Comparisons of duplicate samples analyzed by ICP-MS and IC showed no marked differences (<10%). Overall, the accuracy of elemental data was better than 10% based on repeated measurements of two reference water samples: NIST SRM-1640a (spring water) and SCP ESL-2 (groundwater) (Phan et al., 2018a). Even though the TDS levels of these two reference standards are in similar range of the diluted PW, the difference in sample matrix with PW samples suggests that these standards might not fully represent the best estimate of the accuracy of elemental data, particularly trace metal concentrations. However, no certified reference material is currently available for metal concentration analysis of oil and gas PW (Tasker et al., 2019). Measurement of Fe(II) was performed by the 1,10-phenanthroline colorimetric method, in which a split of the filtered acidified aliquots of the fracturing fluid and PW samples were reacted with an aqueous 1,10-phenanthroline solution and ammonium acetate buffer, and the Fe(II)-1,10-phenanthroline complex was measured at 508 nm per methods reported in Hakala et al. (2009). It is noted that iron colloids formed during PW sample collection likely resulted in underestimated Fe concentrations (Phan et al., 2018a). In addition, Phan et al. (2018a) also demonstrated that colloidal clays liberated from the fractured shale into the <0.45 μm filtered water possibly contributed to Al, Si, and Ti in this fraction. Thus, the interpretation of chemical reactions using Fe, Al, Si, and Ti concentrations should be done with caution as indicated in the discussion.

2.2.2. Water (δ^2H, $\delta^{18}O$) and metal (δ^7Li, $\delta^{11}B$, $^{87}Sr/^{86}Sr$) isotopes

Isotopic compositions of H (δ^2H) and O ($\delta^{18}O$) of water were analyzed at the Stable Isotope Lab at West Virginia University whereas metal isotopes (δ^7Li, $\delta^{11}B$, $^{87}Sr/^{86}Sr$) were measured on a ThermoFisher Neptune Plus multi-collector inductively coupled plasma mass-spectrometer (MC-ICP-MS) at the University of Pittsburgh, USA. For water isotopes ($\delta^{18}O_{H2O}$, δ^2H_{H2O}) duplicate samples were taken by filling a pre-rinsed 8 mL glass threaded vial, with no headspace. Parafilm was wrapped around the lid of the vial and refrigerated until analysis. Samples for δ^2H_{H2O}, $\delta^{18}O_{H2O}$ were analyzed on a Gas Bench II device coupled to a Finnigan Delta V Advantage mass spectrometer at the IsoBioGem Laboratory at West Virginia University. The Gas Bench II device is connected to a GC-PAL auto-sampler that allows for online sample preparation. For analysis, 500 μL of water sample was added to individual flat bottom Labco® 10 mL auto-sampler vials and flushed with a blend of CO_2 in He and H_2 in He equilibrating gas mixture for $\delta^{18}O_{H2O}$ and δ^2H_{H2O} measurement, respectively. The analysis of δ^2H_{H2O} also requires the addition of a platinum catalyst during flushing and equilibration to accelerate exchange processes. The samples were equilibrated for 24 h at 25 °C in the auto-sampler tray. The equilibrated headspace gas in individual vials are transported via a two-port needle of the autosampler to the NAFIONTM trap, Valco valve, injected into PoraPlot Q fused silica GC column and finally transported to the mass spectrometer for isotope measurement. The reproducibility and accuracy were monitored by duplicate analysis of samples and internal lab standards, previously calibrated to international standards, and were better than 0.3‰ for $\delta^{18}O$, and 1.0‰ for δ^2H, respectively. All isotope values are reported in per mil (‰) relative to VSMOW (Vienna Standard Mean Ocean Water).

The analytical technique for Li isotopes (^6Li and ^7Li) followed our previous method (Phan et al., 2016). We note that the cation exchange resin (AG50W-X8, 200–400 mesh) was packed in 6.0 N HCl solution to achieve 2 mL of resin bed. This same amount of resin will be expanded to >2 mL when the resin is rinsed with water. A novel rinsing procedure using 5% NaCl for 1 min was applied after 4 to 6 h of analysis; this

Table 2
Major and minor elements, $^{87}Sr/^{86}Sr$ in leachates of rocks ($n = 35$) recovered from MIP-3H drill core covering the entire vertical portion of Marcellus Shale.

Parameter	Water-soluble fraction[a]		Adsorbed fraction[a]		Carbonate minerals[a]		Whole rock	
	Mean	±2SD ($n = 35$)	Mean	±2SD ($n = 35$)	Mean	±2SD ($n = 35$)	Mean	±2SD ($n = 35$)
Li, ppm	0.6	0.4	0.53	0.36	0.82	0.91	na	na
B, ppm	2.6	1.2	2.3	0.89	4.0	2.2	na	na
Sr, ppm	7.6	4.8	43	17	52	152	294	715
Cl, ppm	908	672	na	na	na	na	na	na
Br, ppm	4.9	3.1	na	na	na	na	na	na
Cl/Br	186	105	na	na	na	na	na	na
Na/Br	187	115	na	na	na	na	na	na
Li/Ca	0.002	0.002	0.0001	0.0002	0.0002	0.0006	na	na
B/Ca	0.009	0.009	0.00005	0.00005	0.001	0.003	na	na
Sr/Ca	0.03	0.01	0.01	0.02	0.002	0.002	0.17	0.29
Li/Na	0.0006	0.0005	0.002	0.002	0.03	0.03	na	na
B/Na	0.003	0.001	0.01	0.01	0.14	0.13	na	na
Sr/Na	0.01	0.01	0.18	0.18	1.00	1.5	0.13	0.57
$^{87}Sr/^{86}Sr$[a]	na	na	0.7115	0.0024	0.7102	0.0032	na	na

na = not available.
[a] Previously reported in Phan et al. (2019).

procedure was shown to effectively wash out Li (Lin et al., 2016) and as observed in this study. Due to the introduction of a high total dissolved solid solution (5% NaCl), the skimmer valve was closed to prevent potential problems with the extraction lenses of the Neptune Plus MC-ICP-MS at the University of Pittsburgh. The measured $^{7}Li/^{6}Li$ ratio is reported as:

$$\delta^{7}Li = \left(\frac{^{7}Li/^{6}Li_{sample}}{^{7}Li/^{6}Li_{LSVEC}} - 1\right) \times 1000\ (‰) \quad (1)$$

where $^{7}Li/^{6}Li_{LSVEC}$ is the average $^{7}Li/^{6}Li$ ratio of SRM–8545 (LSVEC) standard (Li_2CO_3) measured before and after the sample. Long-term replicate measurements of LSVEC by the Neptune Plus MC-ICP-MS yielded a precision of about 0.5‰ (Phan et al., 2016; Phan et al., 2018b). In this study, about 70% of the PW samples were measured in duplicate; two separate aliquots of the same sample were processed through column chemistry and measured for $^{7}Li/^{6}Li$ ratio. The $\delta^{7}Li$ values reported in Table 1 are the average value, and 2SD are two standard deviations of the column duplicate. The measured $\delta^{7}Li$ of WA-A25, an in-house PW sample, was 9.6 ± 0.4 (2SD; $n = 3$) which is consistent with 9.4 ± 0.1 (2SD; $n = 2$) (Macpherson et al., 2014), 9.5 ± 0.4 (2SD; $n = 5$) (Phan et al., 2016); 9.2 ± 0.1 (2SD; $n = 2$) (Phan et al., 2018b). Likewise, measured $\delta^{7}Li$ of seawater (NASS-6) was 31.3 ± 0.7 (2SD, $n = 3$), agreeing well with 30.87 ± 0.15 (Lin et al., 2016).

B isotopes (^{10}B and ^{11}B) in PW samples were separated from the sample matrix using the micro-sublimation method (Wang et al., 2010) which was modified after Gaillardet et al. (2001). A detailed description of the sublimation method is described in the Supporting Material. This technique is particularly suitable for samples with high B concentration (>0.7 mg/L; this study) whereas it might be challenging to obtain reliable data for aqueous samples containing much lower B content (Misra et al., 2014) such as surface waters. The whole procedure was done under a HEPA hood in a clean lab. Briefly, PW was diluted in 2% HNO_3 by volume (Optima™, Fisher Scientific) to obtain the B concentration of about 1 mg/L. A 50 μL aliquot of the sample was pipetted and loaded onto the inner side of the cap of a 5 mL conical bottom PFA vial (Savillex). The vial with the conical-bottom-side up was then closed firmly and placed inside a PTFE rack on a hot plate at 98 °C for 18 h. B was sublimated and condensed at the conical bottom whereas the sample matrix (salts and organic matter) remains as residue on the cap. Purified B was dissolved and diluted in 0.5% HF (Optima™, Fisher Scientific) by weight (1% by volume) to the concentration of 50 μg/L for isotope analysis. The analytical protocol used in this study is similar to Foster (2008) which is described in detail in the Supporting Material. The aqueous solution was introduced to a Neptune Plus MC-ICP-MS at the University of Pittsburgh using an HF-resistant sample introduction system (47 mm PFA PureChamber™ Spray Chamber, sapphire injector, Pt (tip) cone, and Pt skimmer). The measured $^{11}B/^{10}B$ is reported as:

$$\delta^{11}B = \left(\frac{^{11}B/^{10}B_{sample}}{^{11}B/^{10}B_{SRM-951}} - 1\right) \times 1000\ (‰) \quad (2)$$

where $^{11}B/^{10}B_{SRM\text{-}951}$ is the average $^{11}B/^{10}B$ of the SRM-951 (NIST) isotope standard (50 μg/L) measured before and after the sample. The measured $^{11}B/^{10}B$ was corrected for blank (on-peak zero) contribution on individual masses. For each water sample, three aliquots were sublimated and analyzed for $\delta^{11}B$. One was used to check B recovery whereas two were used for isotope analysis. Thus, the $\delta^{11}B$ values reported in Table 1 are the average values and 2SD are two standard deviations of three separate aliquots of the same sample. The procedural blank contribution was <0.003% ($n = 3$) which was negligible. The B recovery of all analyzed PW samples was 103 ± 7% (2SD; $n = 20$). Repeated measurements of SRM-951 yielded $\delta^{11}B = 0.0 \pm 0.5$‰ (2SD; $n = 13$). Likewise, measurements of an in-house standard (single element ICP standard, without going through sublimation) yielded $\delta^{11}B = -0.5 \pm 0.6$‰ (2SD; $n = 13$) to check for day to day consistency of $\delta^{11}B$ measurements. In addition, analyzed $\delta^{11}B$ value of an in-house water reference standard (E44, oil PW from San Andres formation, TX, USA) was 18.3 ± 0.4 (2SD; $n = 4$), following the same micro sublimation and analytical procedure. The accuracy of B isotope analysis is evaluated based on repeated analysis of seawater (NASS-6, NRC Canada) concurrently with PW samples. Our analyzed $\delta^{11}B$ of NASS-6 seawater was 40.3 ± 0.6‰ (2SD; $n = 7$), within the analytical error of seawater $\delta^{11}B$ values: $\delta^{11}B = 39.65 \pm 0.41$‰ (Foster et al., 2013); $\delta^{11}B = 39.87 \pm 0.25$‰ (2SD, $n = 58$) (Louvat et al., 2014). Overall, the accuracy of $\delta^{11}B$ data is estimated to be within 0.5‰.

Radiogenic Sr isotope ratio ($^{87}Sr/^{86}Sr$) were analyzed following a previous procedure (Wall et al., 2013). The analysis was performed using a Neptune Plus MC-ICP-MS at the University of Pittsburgh. The measured $^{87}Sr/^{86}Sr$ was normalized to SRM-987 Sr standard ($^{87}Sr/^{86}Sr = 0.710240$) and reported as ε_{Sr}^{sw} relative to seawater.

$$\varepsilon_{Sr}^{sw} = \left(\frac{^{87}Sr/^{86}Sr_{sample}}{^{87}Sr/^{86}Sr_{seawater}} - 1\right) \times 10000 \quad (3)$$

where $^{87}Sr/^{86}Sr$ seawater is the measured ratio of modern seawater. In this study, we use the value measured at the University of Pittsburgh as the seawater standard: $^{87}Sr/^{86}Sr_{seawater} = 0.709166$ (Chapman et al., 2012). Two reference standards, UD6–120518–S (PW) and EN-1 ($CaCO_3$, shell of giant clam *Tridacna gigas*, USGS standard), were processed in each chemistry session during the study. The in-house standard UD6-120518-S (PW) yielded $^{87}Sr/^{86}Sr = 0.719959 \pm 0.000022$ (2SD; $n = 9$), agreeing well with $^{87}Sr/^{86}Sr = 0.719956 \pm 0.000041$ (2SD; $n = 8$) (Kolesar Kohl et al., 2014; Phan et al., 2016); $^{87}Sr/^{86}Sr = 0.719958 \pm 0.000020$ (2SD; $n = 9$) (Phan et al., 2018b). Likewise, repeated measurement of EN–1 in this study yielded $^{87}Sr/^{86}Sr = 0.709166 \pm 0.000018$ (2SD; $n = 10$), consistent with $^{87}Sr/^{86}Sr = 0.709159 \pm 0.000032$ (2SD, $n = 9$) (Phan et al., 2018b).

2.3. Two end-member mixing model

In the hydraulically fractured Marcellus Shale, three components/end-members that control the evolution of chemical constituents in the PW are (i) fracturing fluid, (ii) in situ formation water, and (iii) reservoir rock minerals. Previous studies demonstrated that mixing between highly saline formation water with early PW is the main process controlling the temporal evolution of the PW chemistry (Capo et al., 2014; Phan et al., 2016; Rowan et al., 2015). The early PW likely represents the fluid that is derived from the chemical reactions between the hydraulic fracturing fluid and minerals in the reservoir during hydraulic fracturing. In this study, we differentiate the chemical reactions between fluid and reservoir rock from fluid mixing by comparing the divergence of the geochemical data from the mixing line due to contribution from the rock end-member (the 3rd component).

The two-component mixing model was used in this study. The concentration and isotopic composition (ratio or δ notation) of the mixture is defined as:

$$C_{mix} = C_1 \cdot f_1 + C_2 \cdot (1 - f_1) \quad (4)$$

$$R_{mix} = \frac{R_1 \cdot (C_1 \cdot f_1)}{C_{mix}} + \frac{R_2 \cdot C_2 \cdot (1 - f_1)}{C_{mix}} \quad (5)$$

where:

C_{mix}, R_{mix} = concentration and isotopic composition, respectively, in the mixture

C_1, R_1 = concentration and isotopic composition, respectively, in end member 1

C_2, R_2 = concentration and isotopic composition, respectively, in end member 2

f_1 = fraction of end member 1 in the mixture.

3. Results

3.1. Concentrations of major and minor ions and total organic carbon

The elemental concentrations are shown in Table S1 (supporting material), and the TDS was calculated as a total of the concentrations of major and minor ions, excluding bicarbonate. The elemental concentrations of 16 out of 54 samples used in this study were previously reported in (Phan et al., 2018a), as indicated in Table S1 (supporting material). This sub data set was reported to discuss the role of colloids in the transport of metals in PW (Phan et al., 2018a). Well MIP-3H and MIP-5H were fractured for a total of 28 stages using freshwater from the Monongahela river. Thus, the TDS of the fracturing fluid from all stages are expected to be similar to those at stage 11 (300 mg/L). This TDS level was about two orders of magnitude lower than the TDS in fracturing fluids of southwestern PA wells (50,000 ± 20,000 mg/L) where recycled PW was used as make-up water (Chapman et al., 2012; Rowan et al., 2015). The concentrations of major and minor elements (Na, K, Mg, Ca, Cl, Br, Sr, Li), likewise TDS, of day-1 PW from MIP-3H and MIP-5H are much higher than the fracturing fluids whose inorganic compositions are nearly identical to the make-up water (Monongahela river water). The increase in these elements occurred linearly to the log of time, clearly observed for MIP-3H (Fig. 2A), but not as clear for well MIP-5H. We also found that the increase in salinity positively and linearly correlated with the cumulated volume of PW of MIP-3H, but not MIP-5H (Fig. S6; Table 1). While the increase in TDS was observed for both wells, the TDS in MIP-5H well increased more rapidly than the TDS in MIP-3H. The highest TDS values of 158,000 mg/L for MIP-3H and 248,000 mg/L for MIP-5H were attained after about 16 months of production, and the last sample analyzed in this study. This TDS level is within the range of TDS levels in formation water (Blondes et al., 2018; Chapman et al., 2012; Rowan et al., 2015) in southwestern and northcentral PA sites (Fig. 1), and other locations in Pennsylvania. The TDS did not plateau over this sampling period, as observed in previous studies (e.g., Rowan et al., 2015; Phan et al., 2016). It is also noted that the concentrations of Ba increased over time, 240 mg/L on the first day to 6600 mg/L after 16 months of production, following the general trend of major and other minor elements listed above. However, unlike the other major/minor elements, no spike of Ba was observed in MIP-3H PW samples collected between day 2 and day 4 (Fig. 2C). Likewise, Ba in PW of MIP-5H remained constant (~600 mg/L) within the first 24 h which contrasts with the decreasing trends of major and minor elements (Fig. 2D). In contrast to major ions, the TOC contents of PW collected on the first few days from MIP-3H were generally higher (>100 mg/L) than those collected later. Overall, the TOC contents did not correlate with time or TDS. Sulfate concentrations in the fracturing fluids of both wells (~130 mg/L) were much higher than PW collected after one month of production which was below the detection limit of 10 mg/L (Fig. 2; Table S1). We found that the detection limits for many trace metals were high due to high salinity

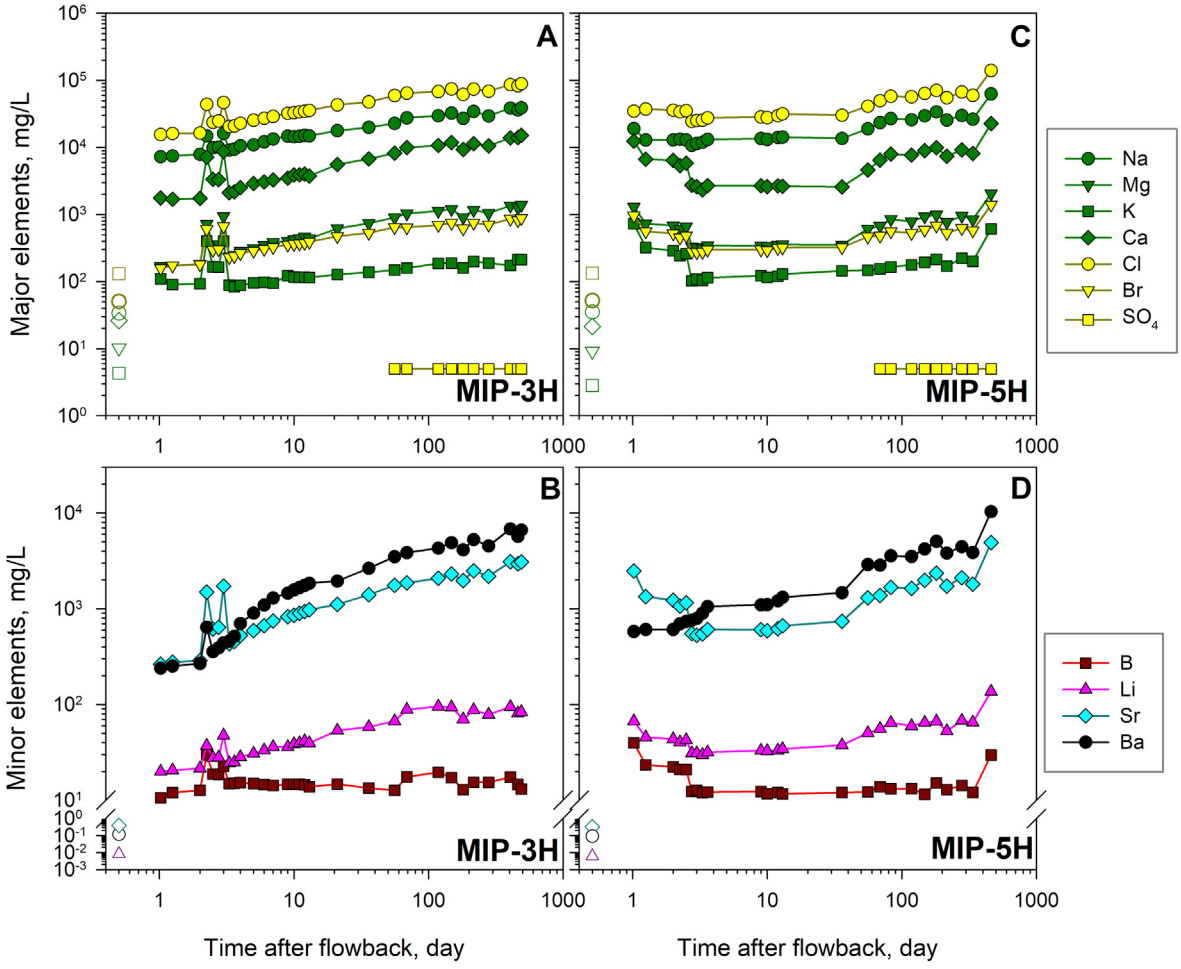

Fig. 2. Changes in the concentrations of major and minor elements in time-series Marcellus Shale PW samples from two horizontal wells at MSEEL field site: well MIP-3H (A, B), well MIP-5H (C, D) over time (number of days from the first day of water flow from the wells). Fracturing fluids from stage 11 of a total of 28 hydraulic fracturing stages of well MIP-3H and MIP-5H, mainly comprising of make-up water from Monongahela river, are shown as open symbols.

that requires large dilution factors, a typical issue experienced by many laboratories reported in Tasker et al. (2019). Matrix separation before ICP-MS analysis can increase the detection limits for trace metals (Jackson et al., 2018). However, this method is time-consuming, thus, only concentrations above the detection limits are used for discussion. While most trace elements in PW were below the analytical detection limits, limited data show that trace metals in early PW were higher than in the fracturing fluid. In both wells, Fe (primarily as Fe(II)) and Zn generally increased over time. The $Fe(II)/Fe_{total}$ ratio in PW is between 0.8 and 1.3 for all of the samples analyzed for Fe(II), and shows a highly variable trend within the first 8 days of production (Table S1). Values for $Fe(II)/Fe_{total} > 1$ may reflect an influence of colloidal phases on iron measurements, the proportion of which may be influenced by sample preparation and dilution techniques applied for colorimetric (Fe(II); dilution only performed on samples with [Fe(II)] > 112 mg/L) versus ICP-MS analysis. Despite these effects, the general observation is that most of the Fe present in the PW samples is in the reduced form.

3.2. Water isotopes (δ^2H, $\delta^{18}O$) in produced waters

The isotopic composition of the make-up water used for mixing with fracturing chemicals prior to injection into MIP-3H and MIP-5H were −8.7‰ for $\delta^{18}O$ and −48.1‰ for δ^2H, and plots slightly to the right of the local meteoric water line (LMWL) (Fig. 3, Table 1). The deviation of the river water away from the LMWL could plausibly be because the precipitation source in this part of West Virginia is often mixed with evaporative and recycled atmospheric moisture originating from the Great Lakes region. The δ^2H and $\delta^{18}O$ values of PW are higher, ranging from −3.4 to −6.3‰ for $\delta^{18}O$ and −45.1 to −30.6‰ for δ^2H (Fig. 3). The range of δ^2H of PW at MSEEL was similar to the range reported for

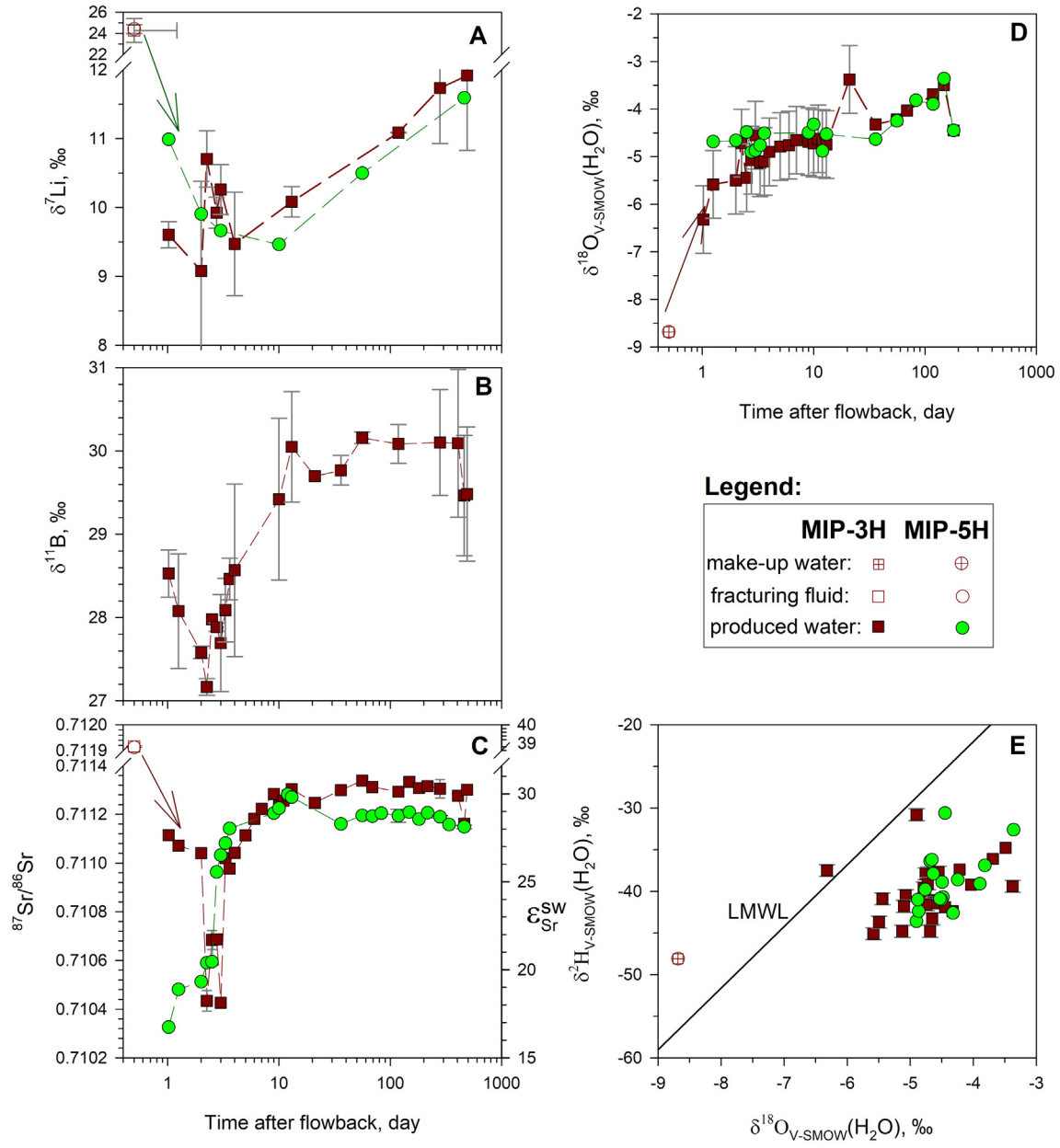

Fig. 3. Changes in the isotopic compositions of Li (δ^7Li; A), B (δ^{11}B; B), Sr ($^{87}Sr/^{86}Sr$; C), and water oxygen ($\delta^{18}O_{V\text{-}SMOW}$; D) in time-series Marcellus Shale PW over time (number of days from the first day of water flow from the wells). The $\delta^{18}O_{V\text{-}SMOW}$ vs. $\delta^2H_{V\text{-}SMOW}$ of water in PW is compared with the local meteoric water line (LMWL; E). The LMWL data are for local surface water (Bowen et al., 2007). Fracturing fluids from stage 11 of a total of 28 hydraulic fracturing stages of well MIP-3H and MIP-5H, mainly comprising of make-up water from Monongahela river, are shown as open symbols.

PW from southwest PA (Rowan et al., 2015). However, $\delta^{18}O$ values of MSEEL PW were slightly lower than those in southwest PA (Rowan et al., 2015). While the $\delta^{2}H$ values fluctuated over the entire sampling period, there was a general increasing trend of $\delta^{18}O$ over time (Fig. 3).

3.3. Metal isotopes ($\delta^{7}Li$, $\delta^{11}B$, $^{87}Sr/^{86}Sr$) in produced waters

The $\delta^{7}Li$ values of the fracturing fluids of MIP-3H and MIP-5H were identical, 24.3‰ and 24.4‰, respectively which were much greater (>13‰) than the $\delta^{7}Li$ values of PW returning from these wells on the first day ($\delta^{7}Li = 9.6$ and 11‰; Table 1). The $\delta^{7}Li$ values of both wells fluctuated in the first 4 days, and then increased over time, reaching the highest value of ~12‰ in the PW collected on the last sampling date (~16 months since the start of returning PW). Interestingly, $\delta^{7}Li$ values in MIP-3H and MIP-5H (Fig. 3A) followed the same trends observed for Li concentrations in the PW (Fig. 2B, D). Together with $\delta^{7}Li$ values (Phan et al., 2016) in Marcellus Shale PW from the southwestern and northcentral PA (Fig. 1), we found that $\delta^{7}Li$ strongly correlates with TDS in PW. The $\delta^{11}B$ values were only analyzed for PW from MIP-3H because of the time constraint of this project. The $\delta^{11}B$ values decreased for about 1‰ within 24 h since the start of returning PW and then increased over time reaching a plateau at $\delta^{11}B = 30 \pm 1$‰ (2SD; $n = 9$; Fig. 3B) on the 10th day. The ε_{Sr}^{SW} values of the fracturing fluids of MIP-3H and MIP-5H are identical ($\varepsilon_{Sr}^{SW} = 39$). For well MIP-3H, a decrease in ε_{Sr}^{SW} for 12 units from the fracturing fluid $\varepsilon_{Sr}^{SW} = 39$ to $\varepsilon_{Sr}^{SW} = 27$ on the first day was observed, continued to decrease to the lowest values of 18, and then increased to a plateau of 30 ± 1.2 (2SD; $n = 14$; Fig. 3C). A spike in Sr (and other elements) occurs in PW collected between day 2 and day 4 corresponds to a dip in ε_{Sr}^{SW}. Likewise, these samples exhibit the lowest $\delta^{11}B$ values among the studied PW samples (Fig. 3B). In contrast to MIP-3H, a larger decrease in ε_{Sr}^{SW} (23 units) was observed for well MIP-5H; otherwise, the temporal trend of ε_{Sr}^{SW} in PW of MIP-5H mimics one of MIP-3H (Fig. 3C). Overall, more fluctuations in major and minor element abundances, $\delta^{18}O$, $\delta^{7}Li$, and ε_{Sr}^{SW} were observed during the first few days, and then increasing to reach a stable chemical composition representing in situ formation water.

3.4. Distribution of Li, B, Sr, and $^{87}Sr/^{86}Sr$ in Marcellus Shale core materials recovered from MIP-3H well

The distributions of Li, B, Sr, and $^{87}Sr/^{86}Sr$ in three easily leachable fractions of core materials from the MIP-3H well rocks are summarized in Table 2. Li is mainly associated with clay minerals, minimally absorbed on mineral surfaces, and low in abundance (<1 ppm) in carbonate cement or concretions within the shale (Phan et al., 2016; this study). In contrast, Sr is present at appreciable levels: 7.6 ± 4.8 ppm, 43 ± 17 ppm, and 52 ± 152 ppm in water-soluble, adsorbed, and carbonate fractions, respectively. Within these pools, carbonate cement contains highly variable concentrations of Sr in which $^{87}Sr/^{86}Sr$ (0.7102 ± 0.0032) is much lower than $^{87}Sr/^{86}Sr$ in the adsorbed fraction (0.7115 ± 0.0024) (Phan et al., 2019). In carbonate cement and concretions within the shale, Li was present at Li/Ca (wt. ratio) of 0.0002 ± 0.0006 which is low and a magnitude lower than B (B/Ca = 0.001 ± 0.003) and Sr (Sr/Ca = 0.002 ± 0.002).

4. Discussion

4.1. Fluid mixing in hydraulically fractured reservoir

Good correlations ($r^2 \geq 0.90$; $n = 54$; Fig. S7 Supporting Material) between Li, Na, Mg, Ca, Sr, Ba, Cl, Br, and thus TDS in PW of MIP-3H and MIP-5H suggest that the concentrations of these elements are primarily controlled by similar process(es) and behave conservatively during the temporal evolution of the PW chemistry. A previous study suggested that diffusion (Balashov et al., 2015) can explain the major changes in elemental concentration in early PW. However, isotopic data from this study and previous studies (Capo et al., 2014; Osselin et al., 2018; Phan et al., 2016; Rowan et al., 2015) demonstrate that actual fluid mixing between the fracturing fluid and highly saline in situ formation water is the process explaining the increase in the concentrations and isotope signatures of the dissolved inorganic constituents in the studied PW. A total volume of 40,300 m^3 fluid was injected into MIP-3H during fracturing. A significant portion (at least 94%) of the injected water remained in the reservoir because only 5.6% (2250 m^3; Table 1) was recovered as PW after 16 months of gas production. The increase in elemental concentrations in PW may be partially associated with filtration of water through low permeability shale formation by a process known as hyperfiltration (Balashov et al., 2015; Kanfar and Clarkson, 2016). As water moves by advection through shales or clays, the rock can act like a reverse osmosis membrane retarding the movement of larger molecules and resulting in a depletion in light isotope in the filtrate (Clark and Fritz, 2013). However, it is unlikely that this process is quick enough to result in a large increase in $\delta^{18}O$ (>2‰ for MIP-3H and >5‰ for MIP-5H) in short fracturing periods which are 34 days for MIP-3H and 43 days for MIP-5H (Fig. 3). Thus, this process could explain the loss of the water from the fracturing fluid in the formation (Balashov et al., 2015), but does not explain the increase in $\delta^{18}O$, $\delta^{7}Li$, and $^{87}Sr/^{86}Sr$ in the PW (this study; Phan et al., 2016). Likewise, water isotope ($\delta^{2}H$, $\delta^{18}O$) exchange reaction between the make-up water and minerals in the shale reservoir is not likely because such a shift in water isotope values requires exchange occurring over much longer timescales. Therefore, increased water isotope values ($\delta^{2}H$, $\delta^{18}O$) over time is a result of mixing with formation water that is most likely connate seawater that has been isotopically modified over millions of years through evaporation and interactions with host rock, as demonstrated in previous works (Rowan et al., 2015; Sharma et al., 2015). Together with previous works on the PW of Marcellus Shale (Capo et al., 2014; Phan et al., 2016; Rowan et al., 2015) and Montney Formation in Alberta, Canada (Osselin et al., 2018), the evolution of isotope compositions of water ($\delta^{2}H$, $\delta^{18}O$), $\delta^{7}Li$, and $^{87}Sr/^{86}Sr$ in PW demonstrates that actual mixing between formation water and fracturing fluid occurs within the hydraulically fractured reservoirs.

The progressively increasing shift of $\delta^{18}O$ and TDS (Fig. 4A) follows a mixing line reflecting that the water in PW is a mixture of fracturing fluid and late PW, which is mainly comprised of in situ formation water. This mixing mechanism is also supported by a strong linear correlation ($r^2 = 0.996$; $r^2 = 0.87$ if excluding the fracturing fluids) between Na/Br and Cl/Br of the fracturing fluid and PW (Fig. 4B). This trend represents the change in PW chemistry toward the highly saline fluid (Na-Cl type water) which is possibly derived from seawater evaporation and subsequently long-term interactions with the reservoir. Like Na/Br, Cl/Br, and water isotope data, the mixing model shows that the temporal changes in $\delta^{7}Li$ vs. Li (Fig. 4C) of PW of both MIP-3H and MIP-5H wells follow the mixing line constructed by using the equations in Section 3.3. Phan et al. (2016) showed that the formationwater is heterogeneous across the basin due to different degrees of diagenesis. For example, formation water (>1 year PW) $\delta^{7}Li$, $^{87}Sr/^{86}Sr$, and TDS in MSEEL are about 12‰, 0.7111–0.7113, 160–250 g/L, respectively (this study) whereas it is about 10‰, 0.7100–0.7117, 150–200 g/L in southwestern PA (Capo et al., 2014; Chapman et al., 2012; Phan et al., 2016), 14–15‰, 0.7094–0.7100, 260–320 g/L in northcentral PA (Phan et al., 2016; Rowan et al., 2015) (Fig. 1), and $\delta^{7}Li$ about 9‰ (>90 day PW) in an unknown location in PA (Warner et al., 2014). Thus, we used the latest (oldest) PW collected from the same well to represent the chemical composition of the local in situ formation water. As the formation water is heterogeneous across a single formation in the subsurface, therefore, information from the same geographic location should be used for interpreting geochemical reactions. The mixing trend is also observed for $\delta^{7}Li$ vs. TDS (Fig. 4D), suggesting that the increase in Li in PW is primarily contributed by Li in the saline formation water. The TDS of saline formation waters recovered from Marcellus Shale gas wells (PW after one-year production) vary across the Appalachian

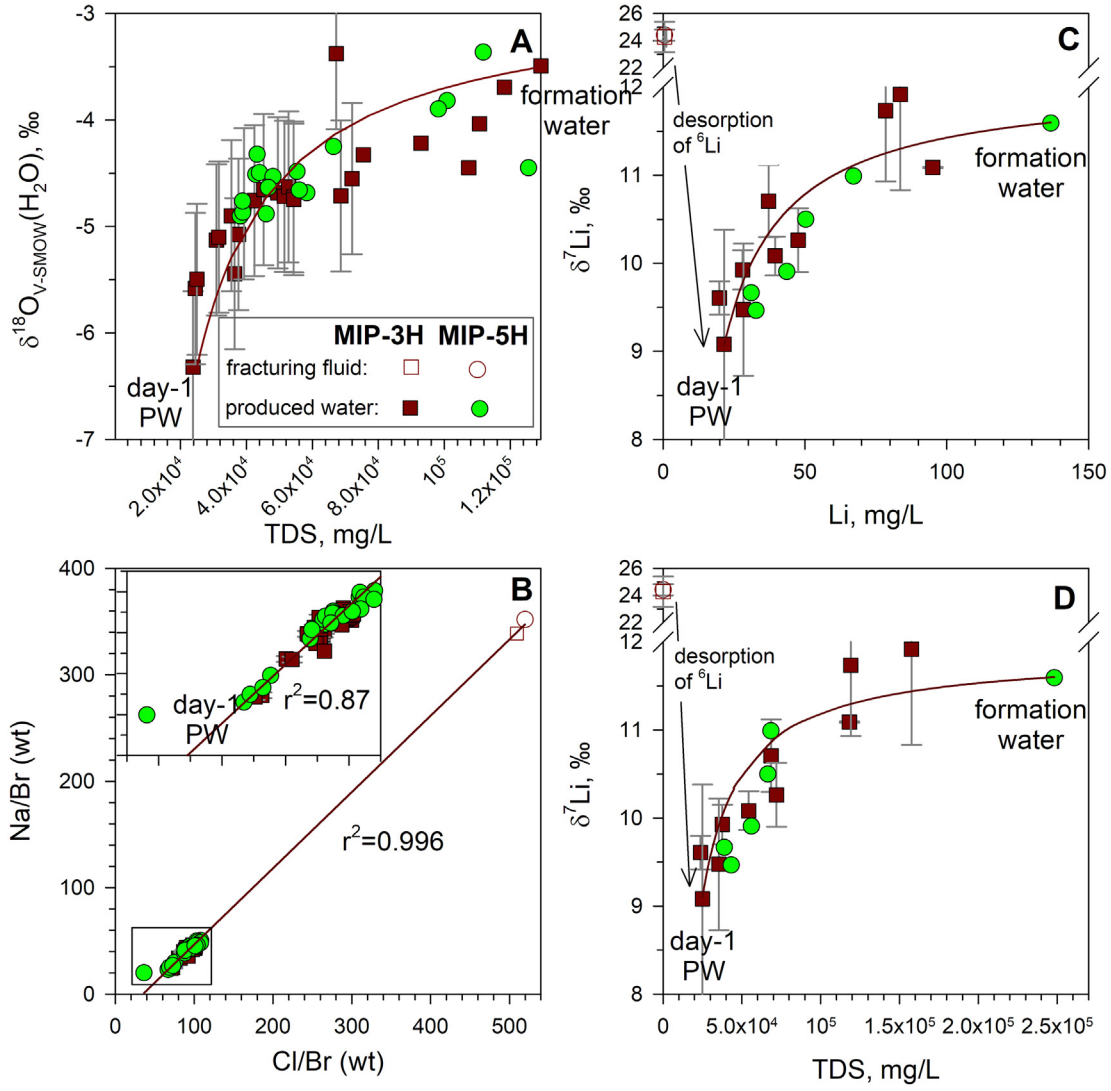

Fig. 4. Variations in the $\delta^{18}O$ vs. TDS (A), Na/Br vs. Cl/Br mass ratio (B), $\delta^{7}Li$ vs. Li (C), and $\delta^{7}Li$ vs. TDS (D) of the fracturing fluid and Marcellus PW of MIP-3H and MIP-5H wells. The inset in B is the blow-out showing the PW data and r^2 value for PW data only. The solid lines in A, C, and D are constructed using a two-end member mixing model (Section 3.3) between day-1 PW and late (>1 year) PW comprising mainly formation water.

Basin (Phan et al., 2016); therefore, the temporal increase in the TDS of PW is dependent on the geographic location of the gas well. Overall, this study demonstrates that mixing between the early fluid and formation water controls the temporal increase in the TDS (major ions), whereas chemical reactions can more significantly affect minor and trace elements in the PW. Therefore, changes in minor and trace metal contents in PW, particularly early PW which are least influenced by formation water, could provide more insight into chemical reactions occurring downhole.

4.2. Geochemical reactions in Marcellus Shale during and post fracturing

Knowledge of water-rock interactions in the fractured reservoir is important for understanding changes in reservoir properties, hydraulic fracturing performance, and PW treatment and disposal. In this section, we discuss the water-rock interactions between fracturing fluid and target reservoir during fracturing and natural gas production (PW sampling period) by assessing the temporal changes of minor and trace metals that do not correlate well with changes in the TDS.

4.2.1. pH driven dissolution – precipitation reactions

Chemical reactions in shale are largely influenced by carbonate dissolution, which buffers the resulting pH in the reservoir (Jew et al., 2017; Pilewski et al., 2019). Marcellus Shale is generally lower in carbonate mineral concentration in comparison to Eagle Ford (2–39%, average = 10%, n = 119) (Chermak and Schreiber, 2014; Hsu and Nelson, 2002). Carbonate content (calcite and dolomite) in Marcellus Shale from MIP-3H core is 6 ± 15% (n = 33), in which calcite is more abundant than dolomite (Phan et al., 2019). Thus, the acid-neutralizing capacity of Marcellus Shale is expected to be much lower compared to other shales if the same amount of acid is used during fracturing. An excessive amount of acid could further lead to clay mineral dissolution. Like hydraulic fracturing of other Marcellus gas wells, hydrochloric acid was used in each of a total of 28 fracturing stages of MIP-3H and MIP-5H wells. In each stage, either 5.7 m^3 (1500 gal) of 7.5% HCl or 11.4 m^3 (3000 gal) of 15% HCl was first pumped downhole to create conduits by dissolving carbonate minerals in the formation, followed by the injection of fracturing fluid, sand, biocides, scale inhibitors, and friction-reducing agents.

A conservative mixing line between the hydraulic fracturing fluid and the carbonate cement end-members shows a dip in $^{87}Sr/^{86}Sr$ in

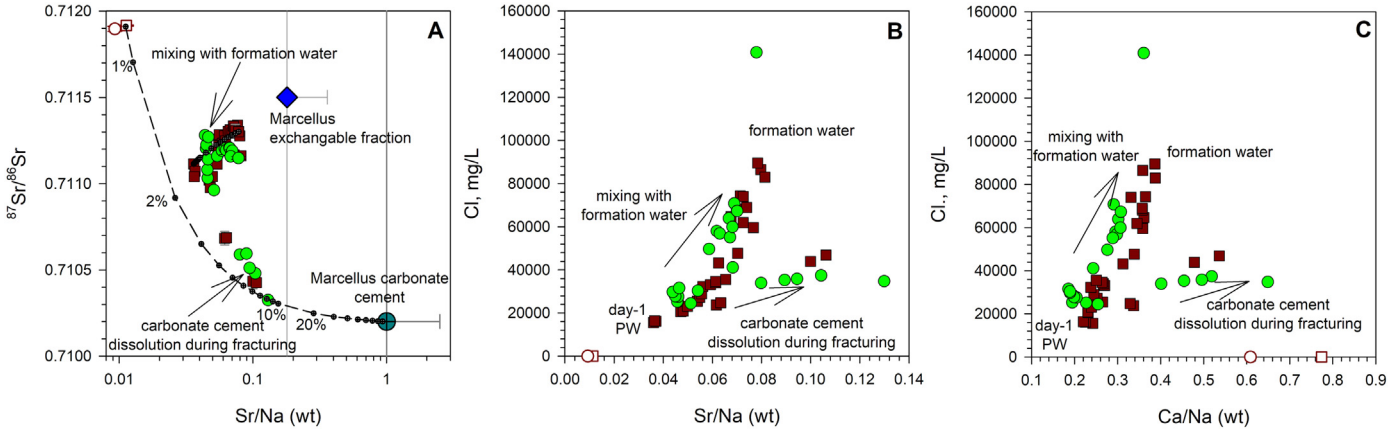

Fig. 5. Variation in $^{87}Sr/^{86}Sr$ vs. Sr/Na (wt) (A), Cl vs. Sr/Na (wt) (B), and Cl (wt) vs. Ca/Na (wt) (C) of the fracturing fluid and Marcellus PW of MIP-3H (filled squares) and MIP-5H wells (filled circles). A dip in $^{87}Sr/^{86}Sr$ toward the dissolution line between the fracturing fluids (open square and circle) and Marcellus carbonate cement reflects the dissolution of carbonate minerals due to the injection of HCl during hydraulic fracturing. Number shown next to the conservative mixing curve (dashed line) represents the theoretical contribution of Sr/Na in the mixture.

early PW (<3 days) toward the dissolution curve (Fig. 5A). This provides evidence for carbonate dissolution of either the cement within the shale or limestones from Cherry Valley formation or both, during the fracturing process. The deviation of $^{87}Sr/^{86}Sr$ demonstrates that the carbonate-reacted fluid is possibly isolated in discrete fractures and is not well mixed with formation water. If this carbonate-reacted fluid is well mixed with in situ formation water, the $^{87}Sr/^{86}Sr$ values in PW are expected to follow the mixing line (Fig. 5A). The Sr/Na of early (≤3 days) PW samples deviated to the right of the linear correlations of Cl vs. Sr/Na (Fig. 5B). A similar relationship was also observed in plots of Cl vs. Ca/Na (Fig. 5C) or Cl vs. B/Na (not shown). The higher Sr/Na, Ca/Na, and B/Na ratios in these samples are likely due to the additional contribution of Sr, Ca, and B from the dissolution of carbonate minerals in the shale by acidic fracturing fluid. This also corroborates with high TOC contents in early PW (Table 1) which is most likely derived from fracturing chemicals.

Li abundance in carbonate minerals in Marcellus Shale is low (<1 ppm; Li/Ca = 0.0002 ± 0.0006; Table 2) and similar to Li levels in the fracturing fluid (<0.01 mg/L; Li/Ca = 0.0003). In contrast, Li/Ca in day-1 PW from MIP-3H and MIP-5H (Table 2) were several magnitudes higher than the Li/Ca in the fracturing fluid suggesting that elevated level of Li in early PW cannot be attributed to carbonate dissolution. This indicates that there must be a significant contribution of Li from other sources such as formation water, as discussed in Section 4.1, chemical additives, clay dissolution, or desorption from clay minerals and organic matter. Adsorption/desorption is discussed in Section 4.2.2.

Marcellus Shale is rich in clay minerals. Illite and muscovite are 30–48% in the Union Springs member (Phan et al., 2019), which is the main target for hydraulic fracturing in Marcellus Shale. Clay dissolution could occur within new stimulated fractures immediately after HCl injection as demonstrated through laboratory experiments (Marcon et al., 2017; Phan et al., 2018b). Based on data from the MIP-3H well, we found a drastic decline in δ^7Li by 14.7‰ from +24.3‰ in the fracturing fluid ([Li] = 0.008 mg/L) to +9.6‰ in the PW returning on the first day ([Li] = 20 mg/L) after the well was unplugged and allowed gas and water to flow. More than three orders of magnitude increase in Li (Fig. 6A) accompanied by a 14.7‰ decline in δ^7Li (Fig. 6B) cannot be solely attributed to clay dissolution or carbonate dissolution.

The δ^7Li values of sedimentary limestone ranging from +6 to +25‰ (Misra and Froelich, 2012), particularly in the Onondaga limestone in the Appalachian Basin (δ^7Li = +13.3 to +15.0‰; Phan et al., 2016) are generally greater than in Marcellus Shale PW. Like other carbonate minerals (Pogge von Strandmann et al., 2013), Li abundance in carbonate cement in Marcellus Shale is low (<1 mg/kg, <2% total Li; Phan et al., 2016). Therefore, the dissolution of carbonate minerals from the reservoir rock cannot explain the low δ^7Li in day-1 PW. To evaluate the role of clay dissolution, we explore the changes in δ^7Li and Li/Al vs. TDS. The δ^7Li in clay minerals is lower than the δ^7Li in the equilibrated fluid due to the preferential uptake of ^6Li primarily into octahedral sites during clay formation (Hindshaw et al., 2019; Pistiner and Henderson, 2003). Li in bulk Marcellus Shale ([Li] = 19–85 mg/kg) is mainly found as structurally bound Li (75–95% of total Li) in silicate minerals such as clays (Phan et al., 2016). Its δ^7Li value ranges between −2.3‰ and +4.3‰ and is up to 26.6‰ lower than δ^7Li value of the fracturing fluid. Laboratory experiments on the partial dissolution of granite showed that ^6Li is preferentially dissolved from secondary minerals within granite, but no significant isotope fractionation is observed during partial dissolution of basalts (Pistiner and Henderson, 2003). If partial dissolution of clay minerals from Marcellus Shale occurred during hydraulic fracturing, the geochemical reaction would introduce more ^6Li into the fluid and therefore induces a decrease in the PW δ^7Li. Isotopically, this explanation corroborates with our field data showing that the δ^7Li in day-1 PW was much lower than δ^7Li in the fracturing fluid.

The dissolution of clays is expected to result in a simultaneous release of Li and Al because Li is mainly held in the structure of clay minerals (Phan et al., 2016). If the dissolution of clays occurred during hydraulic fracturing at MSEEL, then the Li/Al in the PW would inherit the Li/Al in clays with a similar range of Li/Al in whole rock, which is lower than the fracturing fluid by two orders of magnitude. The Li/Al ratios in PW are actually three orders of magnitude higher than Li/Al in the fracturing fluid (Fig. 6B). Therefore, the dissolution of clays is not the main process releasing Li from the shale in the PW. We previously showed that the truly dissolved Al fraction of the PW, as opposed to colloidal fractions <0.45 μm, is significantly lower than reported solution-phase Al concentrations (Phan et al., 2018a). Thus, low levels (<50 μg/L) of "truly dissolved" Al in PW plausibly suggests that clay dissolution did not occur during HCl acid injection.

In summary, pH-driven mineral reactions during hydraulic fracturing at the MSEEL site can be attributed to dissolution of carbonate cement, as shown through the increase in chemical composition (e.g., Sr/Na, Ca/Na, B/Na) and the decrease in $^{87}Sr/^{86}Sr$ ratios in early (<3 days) PW. Carbonate cement is a potentially major source of Sr, Ca, and B in PW, particularly these early PW. Clay dissolution does not contribute significantly to PW chemical signatures observed in this study, however, the ability to characterize secondary precipitation reactions that occur within the reservoir may be affected by multiple factors, including reaction kinetics. The influence of sorption and redox processes on PW chemistry are discussed in the following sections.

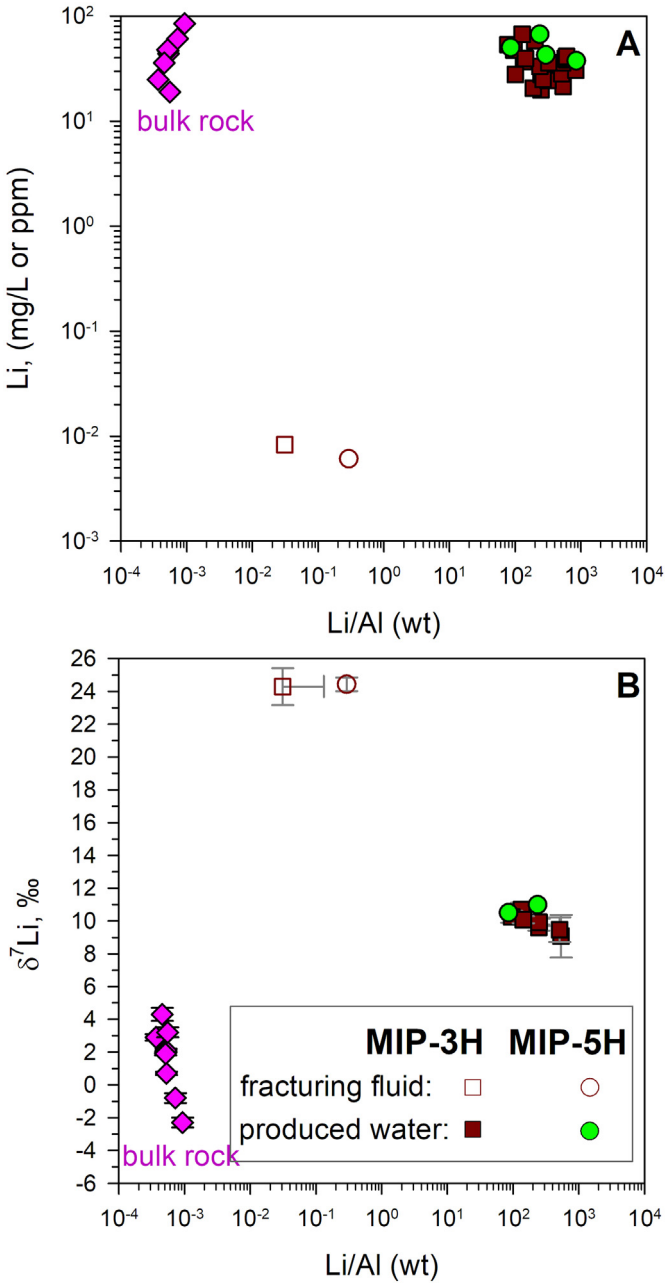

Fig. 6. Variation in Li vs. Li/Al (wt) (A) and δ^7Li vs. Li/Al (wt) (B) of the fracturing fluid and Marcellus PW of MIP-3H and MIP-5H wells. Bulk rock δ^7Li data of Marcellus Shale samples from southwestern and northcentral Pennsylvania, USA (Fig. 1) are from Phan et al. (2016) which are also shown in Table S2 (supporting material).

4.2.2. Adsorption – desorption

Injection of low TDS fracturing fluid into shale reservoirs can cause a change in adsorption-desorption equilibrium of ions in the exchange sites of clays and organic matter. Laboratory studies showed that a significant proportion of Ba in Marcellus Shale is adsorbed on clays and organic matter in Marcellus Shale (Phan et al., 2015; Renock et al., 2016; Stewart et al., 2015) that and can be potentially released into PW via cation exchange. Using field data, our study explores temporal changes in Li, B, δ^7Li, and δ^{11}B relative to the major changes in PW chemistry to evaluate whether desorption during the well shut-in and production contribute to the increase in concentrations of these elements in PW.

Elevated concentration of Li with low δ^7Li value in day-1 PW (20 mg/L, 9.6‰), compared to the fracturing fluid (0.008 mg/L, 24.3‰) and formation water (110 mg/L, ~12‰), suggests ^{6}Li is preferentially released into the fracturing fluid during the well shut-in period. This Li source cannot be the formationwater because Li in formation water at the study area, >1-year PW, is isotopically heavier (δ^7Li ≈ 12‰) than day-1 PW. The enrichment of ^{6}Li in day-1 PW is not likely a result of clay dissolution or carbonate dissolution, as discussed in Section 4.2.1. We hypothesize that the desorption of ^{6}Li from the exchange sites of clay minerals and organic matter could explain the enrichment of ^{6}Li in day-1 PW. To test this hypothesis, we used the sequential extraction data from Phan et al. (2016) (Table 2) and experimentally estimated water-rock ratio of 0.01 from Renock et al. (2016) to calculate an expected Li concentration. Because only 5.6% of the volume of the injected fluid was recovered from MIP-3H well (see Section 4.1), we assume that the fluid loss due to imbibition is as high as 94.4% of the volume of the injected fluid, excluding the contribution of formation water. Mass-balance calculation shows that the theoretically calculated Li derived from desorption of clay minerals and organic matter can result in Li concentration as high as 946 mg/L in PW, a value that can sufficiently explain the Li concentration of 20 mg/L in day-1 PW. Previous studies (Vigier et al., 2008; Zhang et al., 1998) showed that ^{6}Li is preferentially adsorbed on the surface of clay minerals. Therefore, this study suggests that desorption of ^{6}Li from the exchange sites of clays and organic matter in Marcellus Shale during the hydraulic fracturing period is likely the source of ^{6}Li enrichment in early PW (e.g. day-1 PW).

When the wells were unplugged and allowed to flow, both Li and δ^7Li increased over the sampling period and followed the mixing line (Fig. 4D). This suggests that the desorption of Li did not occur throughout the production from the wells or was very negligible even though the high TDS level in PW would favor the desorption process. Like Li, desorption of B from clays would preferentially release ^{10}B, lowering the δ^{11}B in the resulting fluid (Gaillardet and Lemarchand, 2018; Spivack et al., 1987). While δ^7Li progressively increased during the 16-month sampling period, B in PW is relatively unchanged (Fig. 2B) and δ^{11}B in PW quickly reached a relatively constant value of 29.8 ± 0.6‰ (2SD) after 10 days which is 1.8‰ greater than early (<10 days) PW (28.0 ± 0.9‰, 2SD; Fig. 7). The δ^{11}B values in PW were higher than predicted by a conservative mixing curve, plotted using carbonate-reacted PW with the lowest δ^{11}B values (average δ^{11}B = 27.7‰) and PW collected from the same well more than one year in production (average δ^{11}B = 29.7‰; "formation water") end member (Fig. 7). The *t*-test analysis shows that there is a significant difference ($p < 0.01$) between the average δ^{11}B values of these two end-members. This suggests that ^{10}B was preferentially lost over time, which could result from the (1) incorporation of ^{10}B into the clay structures during secondary clay mineral formation or (2) adsorption onto the surface of clays and organic matter, instead of desorption of ^{10}B as suggested by Warner et al. (2014). If secondary clay minerals were formed at an appreciable magnitude, the ratios of the clay forming elements such as Si and Al with Na, presuming Na behaves conservatively, should be lower than expected due to conservative mixing. As shown in Fig. S9 (Supporting Material), Si/Na of PW from both study wells closely follow the mixing line and no change in Al/Na. This observation most likely rules out the hypothesis of B loss due to secondary clay formation. After 10 days, the B isotope signature remained constant (29.8 ± 0.6‰; 2SD), implying that minimal isotope fractionation of B occurred during this period and B was either derived from a constant source or controlled by a single process. In summary, desorption of ^{6}Li from clay minerals during hydraulic fracturing can likely explain the enrichment of ^{6}Li in day-1 PW in comparison to Li in the fracturing fluid. During the production of the well, however, the desorption of Li was unlikely to occur even though PW with high TDS would favor the desorption process. On the other hand, ^{10}B was likely adsorbed on the surface of clays and organic matter in shale, demonstrated by the enrichment of δ^{11}B in comparison to the mixing line (Fig. 7B).

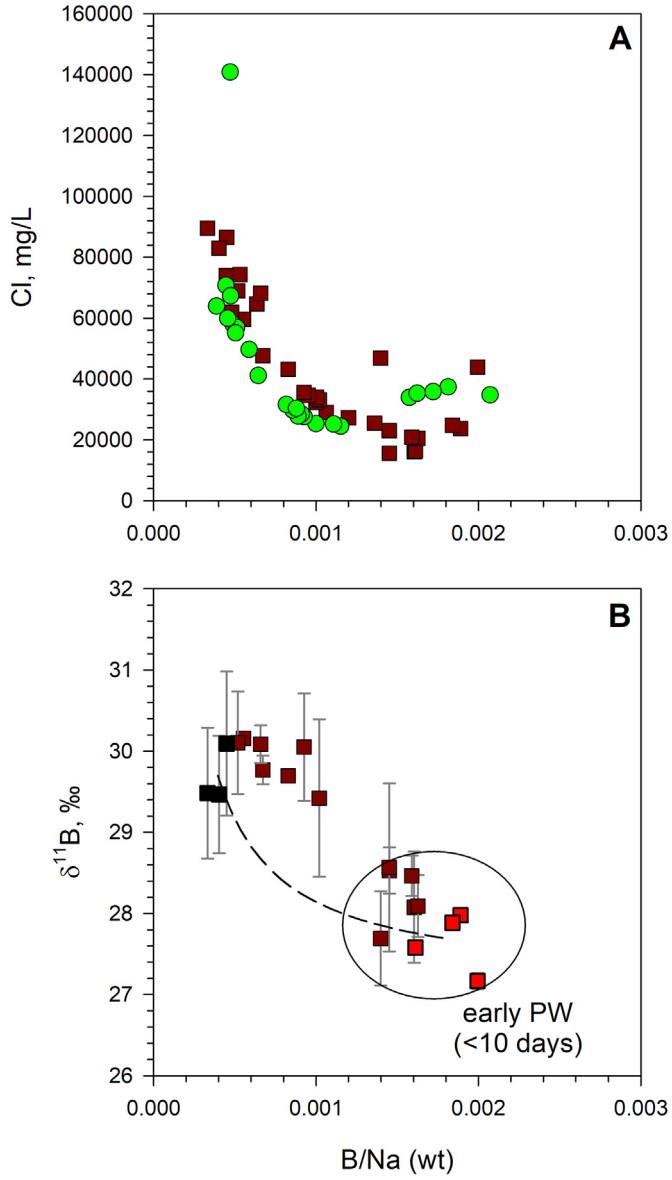

Fig. 7. Variation in Cl vs. B/Na (wt) (A) and $\delta^{11}B$ vs. B/Na (wt) (B) of the Marcellus PW of MIP-3H (filled squares) and MIP-5H (filled circles). The dashed line in B represents conservative mixing between carbonate-reacted PW (light red squares) with formation water (PW collected after one year in production; black squares). (For interpretation of the references to color in this figure legend, the reader is referred to the web version of this article.)

4.2.3. Oxidation reduction reactions

Injection of oxidizing hydraulic fracturing fluid into the shale reservoir could induce/enhance chemical reactions associated with oxidation-reduction (redox) reactions that potentially affect shale porosity and permeability. Barite precipitation could occur due to the release of sulfate from decomposition of gel breaker (e.g., ammonium persulfate) (Matzek and Carter, 2016; Paukert Vankeuren et al., 2017), oxidative dissolution of pyrite (Harrison et al., 2017; Jew et al., 2017; Marcon et al., 2017; Wang et al., 2016), and dissolution of sulfate minerals (e.g., anhydrite) in shale rocks, as suggested for Montney formation in Alberta, Canada (Osselin et al., 2019). The latter is most likely not applicable for Marcellus Shale because both anhydrite and gypsum are not detected (<1%) in shale minerals (Phan et al., 2019). In our two study wells at MSEEL site, the persulfate-based gel breaker, ammonium persulfate, was used during hydraulic fracturing. In addition, pyrite is ubiquitous in the producing portion of the Marcellus Shale at MSEEL site (MIP-3H well). All seven shale samples analyzed contain pyrite, ranging from 1% to 5% (Phan et al., 2019). Previous studies (Chermak and Schreiber, 2014; Stuckman et al., 2019) demonstrated that trace metals are associated with sulfide minerals and organic matter and can be released by oxidative dissolution. Therefore, we hypothesize that redox reactions could play an important role in the temporal evolution of Marcellus PW chemistry, particularly releasing trace metals in early PW. In this section, changes in sulfate, total S, TOC, and redox-sensitive elements such as Fe, Mn, Mo, Co, Ni, and Zn will be examined to elucidate redox reactions in the subsurface.

As shown in Fig. 4B, Cl/Br behaves conservatively, and the increase in Cl/Br in PW is a result of mixing. If the ratios of trace metals over Br exhibit good linear correlations with Cl/Br, fluid mixing is expected to be the primary process driving the changes of trace metals in PW. We found that Total S/Br, Mo/Br, Mn/Br, Zn/Br, and Fe(II)/Br poorly or moderately correlate with Cl/Br (Fig. 8). These poor correlations imply that changes in redox conditions in the subsurface greatly influence the temporal change in trace metals, particularly the redox-sensitive elements. Formation water is in equilibrium with rocks for millions of years under anoxic conditions, given that the depth of fractured Marcellus Shale at the study area was between 2.2 km to 2.3 km. Under the anoxic conditions, it is expected that formation water is low in sulfate, Zn, Mo, and high in Mn based on Eh-pH diagrams of these elements (Langmuir, 1997). We found that trace metals (Cr, Co, Ni, Cu, Zn, Mo) in PW returning from both wells in the first two months are much higher than those in the fracturing fluid (Fig. 9). Therefore, the mixing of the fracturing fluid with formation water does not adequately explain high concentrations of trace elements. Therefore, we suggest that these trace metals could be released by the oxidation of sulfide minerals in the shale rocks. The oxidation could have occurred during the hydraulic fracturing period and continued to occur in the first two months of production. This hypothesis is further supported by the increases in the concentration of total S and Fe(II) in the PW within the first two months.

Total S measured by ICP-OES comprises of sulfur from sulfate and organo-sulfur compounds from fracturing chemicals. Except for the early PW (<10 days) samples derived from carbonate-reacted fluid (See Section 4.2.1), the total S in PW from MIP-3H and MIP-5H generally increases, from 3 mg/L to 20 mg/L (Table S1), during the first two months since the return of the PW. Even though ammonium persulfate, a strong oxidizer (Matzek and Carter, 2016), used in MIP-3H (7.4 mg/kg of fracturing fluid) was about 74 times higher than in MIP-5H, the total S contents (3–20 mg/L) in PW from both wells are in similar range and much lower than the minimally estimated total S (~45 mg/L) in the fracturing fluids. The total S concentration in the fracturing fluid is calculated from the sulfate concentration of ~133 mg/L. In contrast to the major ion concentrations, low total S concentration in day-1 PW (3 mg/L S) suggests that S was removed during the fracturing period. We postulate that either adsorption of ammonium persulfate on shale minerals or precipitation of sulfate derived from persulfate oxidation as gypsum or barite (Hakala et al., 2017; Paukert Vankeuren et al., 2017) or both are the most likely mechanisms for removing sulfur from the system during fracturing period. If the latter hypothesis is valid, oxidation of sulfide-bearing minerals and organic matter in shale by persulfate corroborates with high trace metals in early PW which can be sourced from the oxidation of sulfide minerals. Further evidence for redox-driven reactions involving Fe is shown through the highly-variable concentrations of Fe, which is mostly present as Fe(II), in early PW (<10 days) (Table S1). This suggests that reactions involving both dissolution and precipitation of Fe-bearing phases occur within this time period, which has been observed in laboratory-based experiments (e.g., Marcon et al., 2017; Harrison et al., 2017; Jew et al., 2017), with a longer-term release of Fe over the course of production (Table S1). The longer-term release of Fe could result from continued reactions involving both the shale and steel components of the wellbore, the latter of which involves the production of Fe(II) from the Fe(0) in

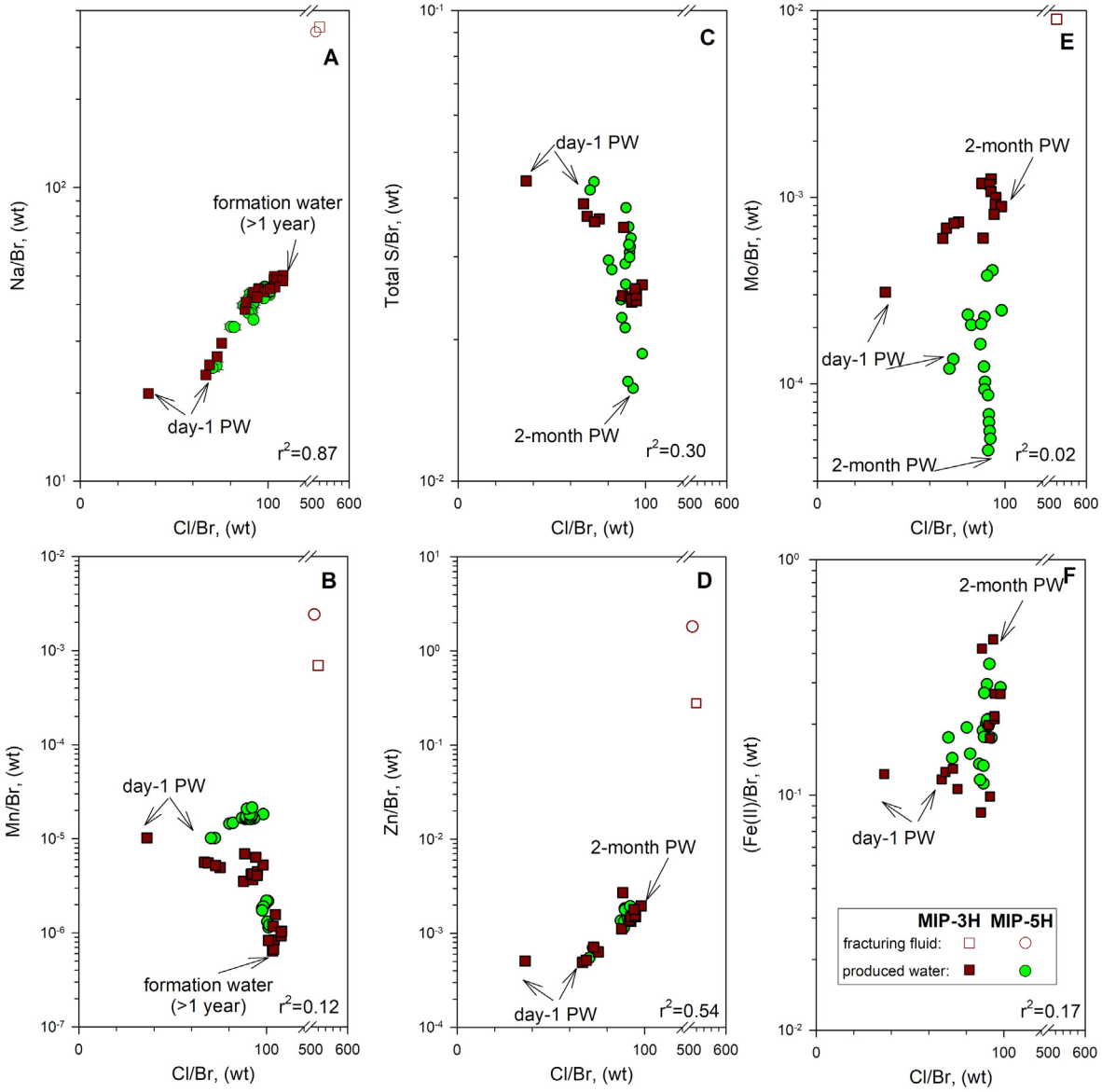

Fig. 8. Variation in varying metal concentrations normalizing to Br vs. Cl/Br in the Marcellus PW of MIP-3H (filled circles) and MIP-5H (filled squares) and fracturing fluids of these two wells (open symbols). The r^2 value at the bottom right corner is for data from both wells.

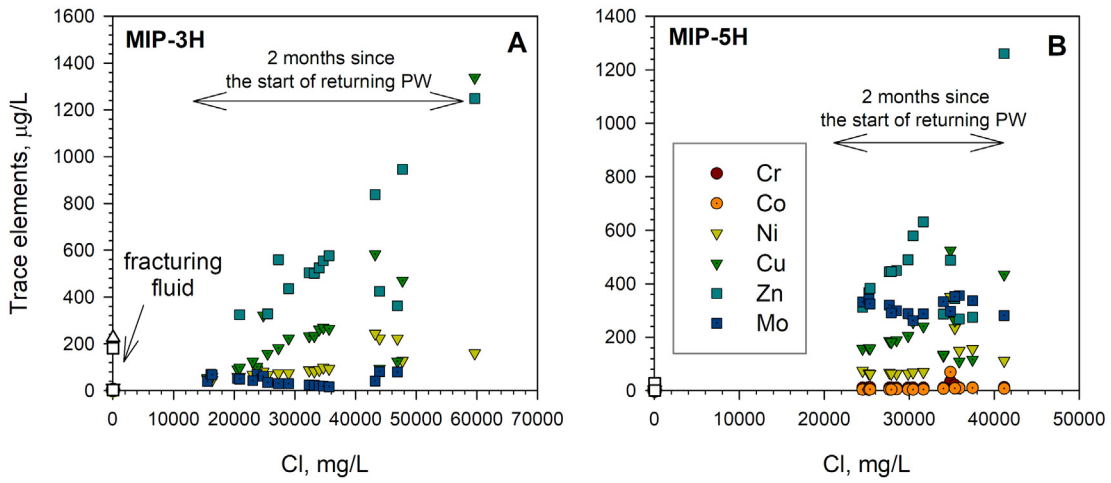

Fig. 9. Variation in trace metal concentrations with Cl in the Marcellus PW of MIP-3H and MIP-5H (filled symbols) and fracturing fluids of these two wells (open symbols).

steel (Popoola et al., 2013). Our data of redox-sensitive constituents in the PW samples collected after two months are limited to sulfate level which is below the detection limit (10 mg/L; Fig. 1). Low sulfate levels imply that bacterial sulfate reduction (Engle and Rowan, 2014) likely occurs under a more reducing environment in the reservoir.

5. Summary

The objective of this study was to apply geochemical proxies in waters produced from a hydraulically-fractured reservoir to characterize water-rock versus fluid mixing reactions within the reservoir. Time-series produced waters from two Marcellus Shale gas wells, fracturing fluid, and rock samples from drill core of the same well were analyzed for metal concentrations and multiple isotopes. Overall, this study demonstrated that concentrations of minor and redox-sensitive metals, and δ^7Li, δ^{11}B, and ^{87}Sr/^{86}Sr in produced waters, can be used to evaluate water-rock interactions in a fracturing fluid-rock-in situ brine system. Major findings regarding water-rock reactions in the subsurface of hydraulically fractured Marcellus Shale are:

- Carbonate dissolution during hydraulic fracturing was evidenced by the distinction in chemical composition (e.g., high Sr/Na, Ca/Na, B/Na, TOC) in early PW and its similarity in ^{87}Sr/^{86}Sr with carbonate cement in Marcellus Shale. An ability to document carbonate dissolution is produced waters demonstrates that geochemical conditions within the reservoir are dynamic enough over a short timeframe that chemically-induced alterations to flow pathways can occur. These observations are consistent with flow pathway alteration observed through carbonate mineral dissolution in laboratory core flood experiments, and the next important step is quantifying how these geochemical changes affect flow within the reservoir.
- Like previous studies, we conclude that the temporal changes in PW chemistry are primarily controlled by actual mixing of fracturing fluid with formation water which could be from within the Marcellus Shale or the adjacent formations. Together with previous studies (e.g., Phan et al., 2016; Rowan et al., 2015), we found that formation water is heterogeneous across the Appalachian Basin. Thus, it is critical to use chemical composition of local formation water for interpreting changes in produced water chemistry in the understanding of sub-surface water-rock reactions and for predicting how these reactions may affect production from unconventional reservoirs. It also is important to consider how mixing between fracturing fluid and formation water affects the predicted chemistry of water produced from onshore unconventional wells that will require treatment and beneficial use.
- Injection of hydraulic fracturing fluid (δ^7Li = 24.3‰) into shale desorbed ^{6}Li from clays and organic matter into PW. This is demonstrated by early PW with δ^7Li (δ^7Li$_{\text{day-1 PW}}$ = 9.6‰) much lower than both the fracturing fluid and local in-situ formation water (δ^7Li = 12‰). These results highlight how clays and organic matter both may contribute reactants to the reservoir fluid-shale system and identifies these components of shale as potentially important contributors to controlling fluid-shale reactions that affect shale permeability.
- High levels of trace elements in early PW demonstrated the oxidation of shale minerals such as sulfides and organic matter, possibly by persulfate, during the hydraulic fracturing period. Then, the fractured shale reservoir moves toward a more reducing environment as demonstrated by low levels of sulfate (below detection limit) in PW collected after 2 months since the start of water return. Dynamic changes in redox conditions coupled with changes in pH throughout the injection-fracturing-shut in-flowback period demonstrates the complexity of geochemical reactions that occur in hydraulically-fractured shale. Documentation of these geochemical changes for active wells also provides a working conceptual model that can be applied to sustainably develop onshore unconventional oil and gas systems.

Declaration of competing interest

The authors declare that they have no known competing financial interests or personal relationships that could have appeared to influence the work reported in this paper.

Acknowledgments

This study was supported by the U.S. Department of Energy, Office of Fossil Energy, as the National Energy Technology Laboratory's ongoing research. Part of the research was also supported by National Science Foundation grant (NSF DEB-1342732) awarded to Sharma. We thank the staff of the Stable Isotope Lab at West Virginia University for collecting the Marcellus PW samples, B. Stewart and R. Capo for providing clean lab space for sample preparation, M. Stuckman for assistance with IC and TOC analysis, C. Hite for assistance with radiogenic Sr isotope analysis, and D. Bain for technical support with ICP-MS analysis. This research was supported in part by an appointment to the National Energy Technology Laboratory Research Participation Program, sponsored by the U.S. Department of Energy and administered by the Oak Ridge Institute for Science and Education (TTP). The manuscript was supported in part by the University of Waterloo start-up grant (TTP).

Disclaimers

Any opinions, findings, conclusions, or recommendations expressed herein are those of the authors and do not necessarily reflect the views of the sponsors. Reference in this paper to any specific commercial product, process, or service is to facilitate understanding and does not imply endorsement by the United States Department of Energy.

Appendix A. Supplementary data

Supplementary data to this article can be found online at https://doi.org/10.1016/j.scitotenv.2020.136867.

References

Akob, D.M., Cozzarelli, I.M., Dunlap, D.S., Rowan, E.L., Lorah, M.M., 2015. Organic and inorganic composition and microbiology of produced waters from Pennsylvania shale gas wells. Appl. Geochem. 60, 116–125.
Balashov, V.N., Engelder, T., Gu, X., Fantle, M.S., Brantley, S.L., 2015. A model describing flowback chemistry changes with time after Marcellus Shale hydraulic fracturing. AAPG Bull. 99, 143–154.
Blauch, M., Myers, R., Moore, T., Lipinski, B., Houston, N., 2009. Marcellus Shale post-frac flowback waters - where is all the salt coming from and what are the implications? SPE Eastern Regional Meeting
Blondes, M.S., Gans, K.D., Engle, M.A., Kharaka, Y.K., Reidy, M.E., Saraswathula, V., Thordsen, J.J., Rowan, E.L., Morrissey, E.A., 2018. U.S. Geological Survey National Produced Waters Geochemical Database (ver. 2.3, January 2018): U.S. Geological Survey Data Release.
Bowen, G.J., Ehleringer, J.R., Chesson, L.A., Stange, E., Cerling, T.E., 2007. Stable isotope ratios of tap water in the contiguous United States. Water Resour. Res. 43.
Burgos, W.D., Castillo-Meza, L., Tasker, T.L., Geeza, T.J., Drohan, P.J., Liu, X., Landis, J.D., Blotevogel, J., McLaughlin, M., Borch, T., 2017. Watershed-scale impacts from surface water disposal of oil and gas wastewater in western Pennsylvania. Environ. Sci. Technol. 51, 8851–8860.
Capo, R.C., Stewart, B.W., Rowan, E.L., Kolesar Kohl, C.A., Wall, A.J., Chapman, E.C., Hammack, R.W., Schroeder, K.T., 2014. The strontium isotopic evolution of Marcellus Formation produced waters, southwestern Pennsylvania. Int. J. Coal Geol. 126, 57–63.
Chapman, E.C., Capo, R.C., Stewart, B.W., Kirby, C.S., Hammack, R.W., Schroeder, K.T., Edenborn, H.M., 2012. Geochemical and strontium isotope characterization of produced waters from Marcellus Shale natural gas extraction. Environ. Sci. Technol. 46, 3545–3553.
Chermak, J.A., Schreiber, M.E., 2014. Mineralogy and trace element geochemistry of gas shales in the United States: environmental implications. Int. J. Coal Geol. 126, 32–44.
Civan, F., 2015. Reservoir Formation Damage. Gulf Professional Publishing.
Clark, I.D., Fritz, P., 2013. Environmental Isotopes in Hydrogeology. CRC press.

Cluff, M.A., Hartsock, A., MacRae, J.D., Carter, K., Mouser, P.J., 2014. Temporal changes in microbial ecology and geochemistry in produced water from hydraulically fractured Marcellus Shale gas wells. Environ. Sci. Technol. 48, 6508–6517.

Engle, M.A., Rowan, E.L., 2014. Geochemical evolution of produced waters from hydraulic fracturing of the Marcellus Shale, northern Appalachian Basin: a multivariate compositional data analysis approach. Int. J. Coal Geol. 126, 45–56.

Engle, M.A., Reyes, F.R., Varonka, M.S., Orem, W.H., Ma, L., Ianno, A.J., Schell, T.M., Xu, P., Carroll, K.C., 2016. Geochemistry of formation waters from the Wolfcamp and "Cline" shales: insights into brine origin, reservoir connectivity, and fluid flow in the Permian Basin, USA. Chem. Geol. 425, 76–92.

Foster, G., 2008. Seawater pH, pCO_2 and $[CO^{2-3}]$ variations in the Caribbean Sea over the last 130 kyr: a boron isotope and B/Ca study of planktic foraminifera. Earth Planet. Sci. Lett. 271, 254–266.

Foster, G.L., Hönisch, B., Paris, G., Dwyer, G.S., Rae, J.W., Elliott, T., Gaillardet, J., Hemming, N.G., Louvat, P., Vengosh, A., 2013. Interlaboratory comparison of boron isotope analyses of boric acid, seawater and marine $CaCO_3$ by MC-ICPMS and NTIMS. Chem. Geol. 358, 1–14.

Gaillardet, J., Lemarchand, D., 2018. Boron in the weathering environment. In: Marschall, H., Foster, G. (Eds.), Boron Isotopes: The Fifth Element. Springer International Publishing, Cham, pp. 163–188.

Gaillardet, J., Lemarchand, D., Göpel, C., Manhès, G., 2001. Evaporation and sublimation of boric acid: application for boron purification from organic rich solutions. Geostand. Geoanal. Res. 25, 67–75.

Ghahfarokhi, P.K., Carr, T., Bhattacharya, S., Elliott, J., Shahkarami, A., Martin, K., 2018. A Fiber-optic Assisted Multilayer Perceptron Reservoir Production Modeling: A Machine Learning Approach in Prediction of Gas Production from the Marcellus Shale, Unconventional Resources Technology Conference, Houston, Texas, 23–25 July 2018. Society of Exploration Geophysicists, American Association of Petroleum …, pp. 3291–3300.

Hakala, J.A., Fimmen, R.L., Chin, Y.-P., Agrawal, S.G., Ward, C.P., 2009. Assessment of the geochemical reactivity of Fe-DOM complexes in wetland sediment pore waters using a nitroaromatic probe compound. Geochim. Cosmochim. Acta 73, 1382–1393.

Hakala, J.A., Crandall, D., Moore, J., Phan, T., Sharma, S., Lopano, C., 2017. Laboratory-Scale Studies on Chemical Reactions Between Fracturing Fluid and Shale Core from the Marcellus Shale Energy and Environmental Laboratory (MSEEL) Site, Unconventional Resources Technology Conference, Austin, Texas, 24–26 July 2017. Society of Exploration Geophysicists, American Association of Petroleum Geologists, Society of Petroleum Engineers, pp. 1458–1467.

Haluszczak, L.O., Rose, A.W., Kump, L.R., 2013. Geochemical evaluation of flowback brine from Marcellus gas wells in Pennsylvania, USA. Appl. Geochem. 28, 55–61.

Harrison, A.L., Jew, A.D., Dustin, M.K., Thomas, D.L., Joe-Wong, C.M., Bargar, J.R., Johnson, N., Brown Jr., G.E., Maher, K., 2017. Element release and reaction-induced porosity alteration during shale-hydraulic fracturing fluid interactions. Appl. Geochem. 82, 47–62.

Hindshaw, R.S., Tosca, R., Goût, T.L., Farnan, I., Tosca, N.J., Tipper, E.T., 2019. Experimental constraints on Li isotope fractionation during clay formation. Geochim. Cosmochim. Acta 250, 219–237.

Hsu, S.-C., Nelson, P.P., 2002. Characterization of eagle ford shale. Eng. Geol. 67, 169–183.

Jackson, S.L., Spence, J., Janssen, D.J., Ross, A., Cullen, J., 2018. Determination of Mn, Fe, Ni, Cu, Zn, Cd and Pb in seawater using offline extraction and triple quadrupole ICP-MS/MS. J. Anal. At. Spectrom. 33, 304–313.

Jew, A.D., Dustin, M.K., Harrison, A.L., Joe-Wong, C.M., Thomas, D.L., Maher, K., Brown Jr., G.E., Bargar, J.R., 2017. Impact of organics and carbonates on the oxidation and precipitation of Iron during hydraulic fracturing of shale. Energy Fuel 31, 3643–3658.

Kanfar, M.S., Clarkson, C.R., 2016. Reconciling flowback and production data: a novel history matching approach for liquid rich shale wells. Journal of Natural Gas Science and Engineering 33, 1134–1148.

Kharaka, Y.K., Maest, A.S., Carothers, W.W., Law, L.M., Lamothe, P.J., Fries, T.L., 1987. Geochemistry of metal-rich brines from central Mississippi Salt Dome basin, U.S.A. Appl. Geochem. 2, 543–561.

King, G.E., 2012. Hydraulic fracturing 101: what every representative, environmentalist, regulator, reporter, investor, university researcher, neighbor and engineer should know about estimating frac risk and improving frac performance in unconventional gas and oil wells. SPE Hydraulic Fracturing Technology Conference. Society of Petroleum Engineers.

Kolesar Kohl, C.A., Capo, R.C., Stewart, B.W., Wall, A.J., Schroeder, K.T., Hammack, R.W., Guthrie, G.D., 2014. Strontium Isotopes Test Long-Term Zonal Isolation of Injected and Marcellus Formation Water after Hydraulic Fracturing. Environ. Sci. Technol. 48, 9867–9873.

Langmuir, D., 1997. Aqueous Environmental Geochemistry. Prentice Hall, Upper Saddle River New Jersey.

Lin, J., Liu, Y., Hu, Z., Yang, L., Chen, K., Chen, H., Zong, K., Gao, S., 2016. Accurate determination of lithium isotope ratios by MC-ICP-MS without strict matrix-matching by using a novel washing method. J. Anal. At. Spectrom. 31, 390–397.

Louvat, P., Moureau, J., Paris, G., Bouchez, J., Noireaux, J., Gaillardet, J., 2014. A fully automated direct injection nebulizer (d-DIHEN) for MC-ICP-MS isotope analysis: application to boron isotope ratio measurements. J. Anal. At. Spectrom. 29, 1698–1707.

Luek, J.L., Harir, M., Schmitt-Kopplin, P., Mouser, P.J., Gonsior, M., 2018. Organic sulfur fingerprint indicates continued injection fluid signature 10 months after hydraulic fracturing. Environmental Science: Processes & Impacts.

Macpherson, G.L., Capo, R.C., Stewart, B.W., Phan, T.T., Schroeder, K., Hammack, R.W., 2014. Temperature-dependent Li isotope ratios in Appalachian Plateau and Gulf Coast Sedimentary Basin saline water. Geofluids 14, 419–429.

Marcon, V., Joseph, C., Carter, K.E., Hedges, S.W., Lopano, C.L., Guthrie, G.D., Hakala, J.A., 2017. Experimental insights into geochemical changes in hydraulically fractured Marcellus Shale. Appl. Geochem. 76, 36–50.

Matzek, L.W., Carter, K.E., 2016. Activated persulfate for organic chemical degradation: a review. Chemosphere 151, 178–188.

Misra, S., Froelich, P.N., 2012. Lithium isotope history of Cenozoic seawater: changes in silicate weathering and reverse weathering. Science 335, 818–823.

Misra, S., Owen, R., Kerr, J., Greaves, M., Elderfield, H., 2014. Determination of δ11B by HR-ICP-MS from mass limited samples: application to natural carbonates and water samples. Geochim. Cosmochim. Acta 140, 531–552.

Orem, W., Varonka, M., Crosby, L., Haase, K., Loftin, K., Hladik, M., Akob, D.M., Tatu, C., Mumford, A., Jaeschke, J., Bates, A., Schell, T., Cozzarelli, I., 2017. Organic geochemistry and toxicology of a stream impacted by unconventional oil and gas wastewater disposal operations. Appl. Geochem. 80, 155–167.

Osselin, F., Nightingale, M., Hearn, G., Kloppmann, W., Gaucher, E., Clarkson, C.R., Mayer, B., 2018. Quantifying the extent of flowback of hydraulic fracturing fluids using chemical and isotopic tracer approaches. Appl. Geochem. 93, 20–29.

Osselin, F., Saad, S., Nightingale, M., Hearn, G., Desaulty, A.M., Gaucher, E.C., Clarkson, C.R., Kloppmann, W., Mayer, B., 2019. Geochemical and sulfate isotopic evolution of flowback and produced waters reveals water-rock interactions following hydraulic fracturing of a tight hydrocarbon reservoir. Sci. Total Environ. 687, 1389–1400.

Ouyang, B., Akob, D.M., Dunlap, D., Renock, D., 2017. Microbially mediated barite dissolution in anoxic brines. Appl. Geochem. 76, 51–59.

Ouyang, B., Renock, D., Akob, D.M., 2018. Effects of organic ligands and background electrolytes on barite dissolution. Geochim. Cosmochim. Acta 256, 6–19.

Patzek, T.W., Male, F., Marder, M., 2013. Gas production in the Barnett Shale obeys a simple scaling theory. Proc. Natl. Acad. Sci. U. S. A. 110, 19731–19736.

Paukert Vankeuren, A.N., Hakala, J.A., Jarvis, K., Moore, J.E., 2017. Mineral reactions in shale gas reservoirs: barite scale formation from reusing produced water as hydraulic fracturing fluid. Environ. Sci. Technol. 51, 9391–9402.

Pearce, J.K., Turner, L., Pandey, D., 2018. Experimental and predicted geochemical shale-water reactions: Roseneath and Murteree shales of the Cooper Basin. Int. J. Coal Geol. 187, 30–44.

Pfister, S., Capo, R.C., Stewart, B.W., Macpherson, G.L., Phan, T.T., Gardiner, J.B., Diehl, J.R., Lopano, C.L., Hakala, J.A., 2017. Geochemical and lithium isotope tracking of dissolved solid sources in Permian Basin carbonate reservoir and overlying aquifer waters at an enhanced oil recovery site, northwest Texas, USA. Appl. Geochem. 87, 122–135.

Phan, T.T., Capo, R.C., Stewart, B.W., Graney, J.R., Johnson, J.D., Sharma, S., Toro, J., 2015. Trace metal distribution and mobility in drill cuttings and produced waters from Marcellus Shale gas extraction: uranium, arsenic, barium. Appl. Geochem. 60, 89–103.

Phan, T.T., Capo, R.C., Stewart, B.W., Macpherson, G., Rowan, E.L., Hammack, R.W., 2016. Factors controlling Li concentration and isotopic composition in formation waters and host rocks of Marcellus Shale, Appalachian Basin. Chem. Geol. 420, 162–179.

Phan, T.T., Bain, D.J., Hakala, A.J., 2018a. Influence of colloids on metal concentrations and radiogenic strontium isotopes in groundwater and oil and gas-produced waters. Appl. Geochem. 95, 85–96.

Phan, T.T., Paukert Vankeuren, A.N., Hakala, J.A., 2018b. Roles of water–rock interactions in the geochemical evolution of Marcellus Shale produced waters. Int. J. Coal Geol. 191, 95–111.

Phan, T.T., Hakala, J.A., Lopano, C.L., Sharma, S., 2019. Rare earth elements and radiogenic strontium isotopes in carbonate minerals reveal diagenetic influence in shales and limestones in the Appalachian Basin. Chem. Geol. 509, 194–212.

Pilewski, J., Sharma, S., Agrawal, V., Hakala, J.A., Stuckman, M.Y., 2019. Effect of maturity and mineralogy on fluid-rock reactions in the Marcellus Shale. Environmental Science: Processes & Impacts 21, 845–855.

Pistiner, J.S., Henderson, G.M., 2003. Lithium-isotope fractionation during continental weathering processes. Earth Planet. Sci. Lett. 214, 327–339.

Pogge von Strandmann, P.A.E., Jenkyn, H.C., Woodfine, R.G., 2013. Lithium isotope evidence for enhanced weathering during oceanic anoxic event 2. Nat. Geosci. 6, 668–672.

Popoola, L.T., Grema, A.S., Latinwo, G.K., Gutti, B., Balogun, A.S., 2013. Corrosion problems during oil and gas production and its mitigation. International Journal of Industrial Chemistry 4, 35.

Renock, D., Landis, J.D., Sharma, M., 2016. Reductive weathering of black shale and release of barium during hydraulic fracturing. Appl. Geochem. 65, 73–86.

Rosenblum, J., Nelson, A.W., Ruyle, B., Schultz, M.K., Ryan, J.N., Linden, K.G., 2017. Temporal characterization of flowback and produced water quality from a hydraulically fractured oil and gas well. Sci. Total Environ. 596–597, 369–377.

Rowan, E.L., Engle, M.A., Kirby, C.S., Kraemer, T.F., 2011. Radium Content of Oil- and Gas-Field Produced Waters in the Northern Appalachian Basin (USA): Summary and Discussion of Data. US Department of the Interior, US Geological Survey, Reston, Virginia.

Rowan, E.L., Engle, M.A., Kraemer, T.F., Schroeder, K.T., Hammack, R.W., Doughten, M.W., 2015. Geochemical and isotopic evolution of water produced from Middle Devonian Marcellus Shale gas wells, Appalachian Basin, Pennsylvania. AAPG Bull. 99, 181–206.

Sharma, S., Bowman, L., Schroeder, K., Hammack, R., 2015. Assessing changes in gas migration pathways at a hydraulic fracturing site: example from Greene County, Pennsylvania, USA. Appl. Geochem. 60, 51–58.

Spivack, A.J., Palmer, M.R., Edmond, J.M., 1987. The sedimentary cycle of the boron isotopes. Geochim. Cosmochim. Acta 51, 1939–1949.

Stewart, B.W., Chapman, E.C., Capo, R.C., Johnson, J.D., Graney, J.R., Kirby, C.S., Schroeder, K.T., 2015. Origin of brines, salts and carbonate from shales of the Marcellus Formation: evidence from geochemical and Sr isotope study of sequentially extracted fluids. Appl. Geochem. 60, 77–88.

Stuckman, M.Y., Lopano, C.L., Berry, S.M., Hakala, J.A., 2019. Geochemical solid characterization of drill cuttings, core and drilling mud from Marcellus Shale Energy development. Journal of Natural Gas Science and Engineering 68, 102922.

Tasker, T.L., Piotrowski, P.K., Dorman, F.L., Burgos, W.D., 2016. Metal associations in Marcellus shale and fate of synthetic hydraulic fracturing fluids reacted at high pressure and temperature. Environ. Eng. Sci. 33, 753–765.

Tasker, T.L., Burgos, W.D., Ajemigbitse, M.A., Lauer, N.E., Gusa, A.V., Kuatbek, M., May, D., Landis, J.D., Alessi, D.S., Johnsen, A.M., 2019. Accuracy of methods for reporting inorganic element concentrations and radioactivity in oil and gas wastewaters from the Appalachian Basin, US based on an inter-laboratory comparison. Environmental Science: Processes & Impacts 21, 224–241.

Vigier, N., Decarreau, A., Millot, R., Carignan, J., Petit, S., France-Lanord, C., 2008. Quantifying Li isotope fractionation during smectite formation and implications for the Li cycle. Geochim. Cosmochim. Acta 72, 780–792.

Wall, A.J., Capo, R.C., Stewart, B.W., Phan, T.T., Jain, J.C., Hakala, J.A., Guthrie, G.D., 2013. High throughput method for Sr extraction from variable matrix waters and 87Sr/86Sr isotope analysis by MC-ICP-MS. J. Anal. At. Spectrom. 28, 1338–1344.

Wang, B.-S., You, C.-F., Huang, K.-F., Wu, S.-F., Aggarwal, S.K., Chung, C.-H., Lin, P.-Y., 2010. Direct separation of boron from Na-and Ca-rich matrices by sublimation for stable isotope measurement by MC-ICP-MS. Talanta 82, 1378–1384.

Wang, L., Burns, S., Giammar, D.E., Fortner, J.D., 2016. Element mobilization from Bakken shales as a function of water chemistry. Chemosphere 149, 286–293.

Warner, N.R., Christie, C.A., Jackson, R.B., Vengosh, A., 2013. Impacts of shale gas wastewater disposal on water quality in Western Pennsylvania. Environ. Sci. Technol. 47, 11849–11857.

Warner, N.R., Darrah, T.H., Jackson, R.B., Millot, R., Kloppmann, W., Vengosh, A., 2014. New tracers identify hydraulic fracturing fluids and accidental releases from oil and gas operations. Environ. Sci. Technol. 48, 12552–12560.

Wenzlick, M., Siefert, N., Hakala, A., 2018. Tailoring Treated Brines for Reuse Scenarios, Unconventional Resources Technology Conference, Houston, Texas, 23–25 July 2018. Society of Exploration Geophysicists, American Association of Petroleum …, pp. 2398–2417.

Whitacre, J.V., 2014. Carnegie Museum of Natural History Pennsylvania Unconventional Natural Gas Wells Geodatabase (v.2014-Q4) [Computer File]. Carnegie Museum of Natural History, Pittsburgh, PA http://www.carnegiemnh.org/science/default.aspx?id=18716 (accessed 13.07.14).

Zhang, L., Chan, L.-H., Gieskes, J.M., 1998. Lithium isotope geochemistry of pore waters from ocean drilling program sites 918 and 919, Irminger Basin. Geochim. Cosmochim. Acta 62, 2437–2450.

Zolfaghari, A., Dehghanpour, H., Noel, M., Bearinger, D., 2016. Laboratory and field analysis of flowback water from gas shales. Journal of Unconventional Oil and Gas Resources 14, 113–127.